Stratigraphic architecture, sedimentology and structure of the Middle Pleistocene Corinth Canal (Greece)

Basile Caterina, Romain Rubi* and Aurélia Hubert-Ferrari

Department of Geography, Faculty of Sciences, Liège University, Quartier Agora, Allée du six Aout 17B, B-4000 Liège, Belgium

BC, 0000-0002-3153-5820; RR, 0000-0001-9627-0432; AH-F, 0000-0001-6381-1415
*Correspondence: romain.rubi@uliege.be

Abstract: The artificial Corinth Canal connects the Aegean Sea with the Corinth Gulf, and displays high steep walls that enable the study of the sedimentological structure of this area. A former strait naturally connecting the gulf with the Aegean Sea is assumed to have existed in this area. Therefore, this exceptionally well-exposed site could be used as an analogue to study tidal straits after its stratigraphic architecture, sedimentology and structure have been defined. To do so, we used field observations associated with a 3D model built using drone imaging. We document a strait divided into a central zone and two adjacent dune-bedded strait zones. The centre is an active horst where sediment bypass occurred. On both sides of this, opposite-dipping conglomeratic dunes are represented by simple- and compound-dune foreset architectures with multiscale asymmetrical herringbone cross-stratifications. These observations document a tidal strait with conglomeratic dune-bedded strait zones in a micro-tidal context. These *c.* 300 ka strait deposits are the only ones preserved in the canal area. After deposition ended, this connection disappeared due to regional uplift and the offset of the Kalamaki–Isthmia Fault. This palaeostrait helps to improve our understanding of Middle–Late Pleistocene palaeogeography and the structural controls on sea connections.

Straits are crucial to the evolution of sedimentary basins because they control the connection between adjacent basins. Depending on the depth of the sill, the isolated basin may experience dramatic changes in its environment in terms of water, sediments and biotas due to glacio-eustatic variations (Nicholls and Russell 1990; Aberhan 2002; Guerra-Garcia *et al.* 2009; Krijgsman *et al.* 2018). Moreover, the sill depth is sensitive to vertical motion linked to faults or regional uplift. In the case of rift basins, it is almost impossible to preserve the sill area due to tectonic activity and erosion. The location and persistence of these connections are often suggested in basin evolution but are rarely documented due to their ephemeral nature. As a result, their sedimentological processes are undercharacterized.

Indeed, even though present-day tidal strait studies allow a picture of the tidal hydrological and sedimentological dynamics to be captured, studies based on outcrops and subsurface data are crucial in extending the limitations of human timescale observations and for considering the long-term geological timescale (Longhitano and Chiarella 2020). To achieve this goal, we have studied the Corinth Canal, which is presently located between the Corinth Gulf and the Aegean Sea in Greece (Fig. 1). This 6.4 km-long and *c.* 21 m-wide canal, dug in 1893, cuts the Isthmus of Corinth and separates the Peloponnese from the Greek mainland. Its steep walls crop out up to 80 m high in the central part and constitute a basin-scale Pleistocene geological cross-section in the active Corinth Rift.

In this paper we investigate the Corinth Canal sections using sedimentological field observations combined with a 3D photogrammetric model to combine the facies and basin scales. These data enable us to highlight and quantify the stratigraphic architecture, sedimentology and structure of the Corinth Canal area during the Pleistocene.

Geological setting

The Corinth Rift (Greece) is the most active European rift, with a present-day extension rate of 1.5 cm a^{-1} (Briole *et al.* 2000). The Corinth Rift is opening the narrow deep Corinth Gulf (120 km long, 40 km wide and 900 m deep), and separates the Greek mainland to the north from the Peloponnese to the south (Fig. 1). The evolution of the Corinth Rift is rather well constrained (Ori 1989; Taylor *et al.* 2011; Ford *et al.* 2013; Nixon *et al.* 2016; Rohais and Moretti 2017; Gawthorpe *et al.* 2018; McNeill *et al.* 2019) and can be divided into three phases (Rohais *et al.* 2007): (1) an initiation phase dominated by a small extension, and a continental and lacustrine sedimentation called 'the Lower Group'; (2) an increase in fault activity associated with the connection of the basins, leading to a transition from deep-water lacustrine sedimentation to a

From: Rossi, V. M., Longhitano, S., Olariu, C. and Chiocci, F. (eds) *Straits and Seaways: Controls, Processes and Implications in Modern and Ancient Systems*. Geological Society, London, Special Publications, **523**, https://doi.org/10.1144/SP523-2021-143

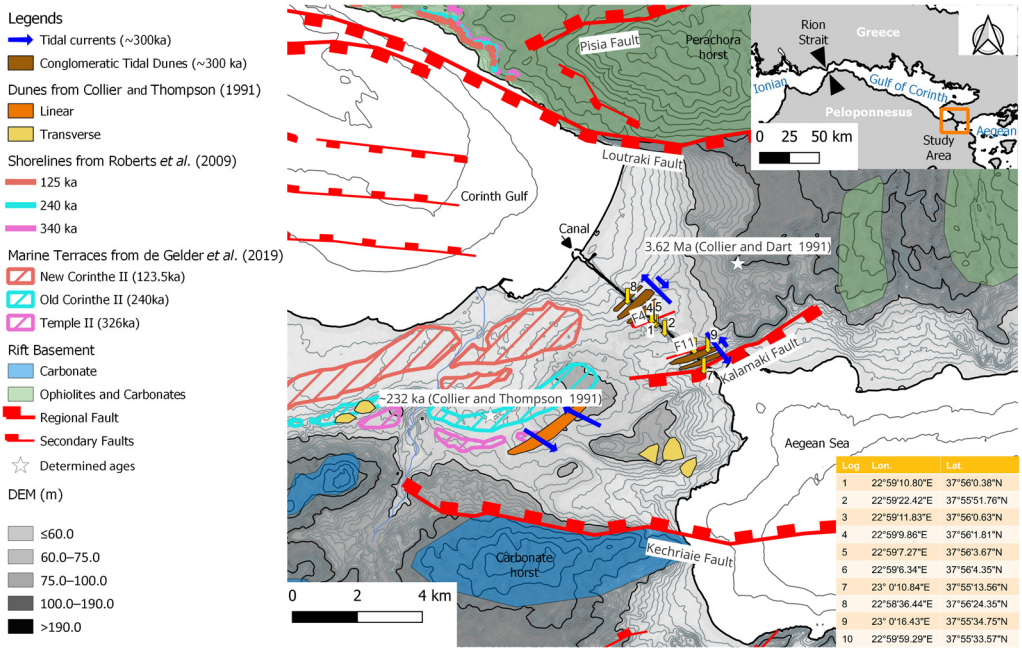

Fig. 1. Map of the Corinth Isthmus with elevations from the European Digital Elevation Model (EU-DEM), version 1.1 (data available at https://land.copernicus.eu/imagery-in-situ/eu-dem/eu-dem-v1.1) and the position of the logged sections along the Corinth Canal. The basement and faults are compiled from Pallikarakis *et al.* (2018) and Fernández-Blanco *et al.* (2019), and the marine terraces are from de Gelder *et al.* (2019).

marine sedimentation referred to as 'the Middle Group'; and (3) exhumation of the synrift deposits on the southern shore by the uplift of the Peloponnese and the northward shift of the deltaic systems, which has been occurring since 1 Ma. Over the last phase, the rift-basin environment has been interpreted as alternating between marine conditions during interglacial/highstand periods and isolated from open-ocean conditions during glacial/lowstand periods as the eustatic sea level fluctuated relative to the elevation of the boundaries of the basin (Sachpazi *et al.* 2003; Bell *et al.* 2008; Taylor *et al.* 2011; Nixon *et al.* 2016). For at least 200 kyr, the sills at the western end of the Corinth Gulf have controlled the connection with the Ionian Sea (Perissoratis *et al.* 2000; Ford *et al.* 2013; Beckers *et al.* 2016). Older and previous connections with the Aegean Sea have been identified to the east at the location of the Corinth Isthmus (von Freyberg 1973; Collier 1990; Collier and Dart 1991). The Corinth Isthmus is a *c.* 10 km-wide corridor bounded by the Loutraki Fault to the north and the Kechriaie Fault to the south (Fig. 1). In the north, the Loutraki peninsula consists mainly of rift basement made of flysch, cherts limestones and ophiolites. On the opposite south border, the Corinth Isthmus consists of a limestone horst.

The Corinth Canal provides a basin-scale outcrop, 6.4 km long and up to 80 m high, that can be used to study the connection between the Corinth Gulf and the Aegean Sea thanks to the uplift in this area, which has occurred at an average minimum rate of 0.3 m ka^{-1} over the past *c.* 205 kyr (Collier 1990). The Corinth Canal section shows a central horst and an adjacent graben called Isthmia (Fig. 2) (Collier 1990) separated by the Kalamaki–Isthmia normal fault to the SE (Papanikolaou *et al.* 2015; Pallikarakis *et al.* 2018). Second-order normal faults cut the strata with offsets of several metres (Collier 1990). The sedimentary evolution of the canal section is revealed by sequences that comprise lower Pleistocene lacustrine Corinth Marls at the base (*sensu* Collier 1990) that are overlain by marine tidal sediments (von Freyberg 1973). These middle–upper Pleistocene marine sediments have been interpreted and subdivided into five transgressive subsequences: wave-reworked conglomerates (first) and beach–shoreface sandstones (second and third); oolitic calcarenites (fourth); and fluvial deposits and soils (fifth). These five subsequences have been tied to major eustatic sea-level fluctuations with a periodicity of *c.* 100 kyr (Collier 1990). In the SE part of the canal (i.e. in the Isthmia Graben), boreholes studies have highlighted conglomeratic

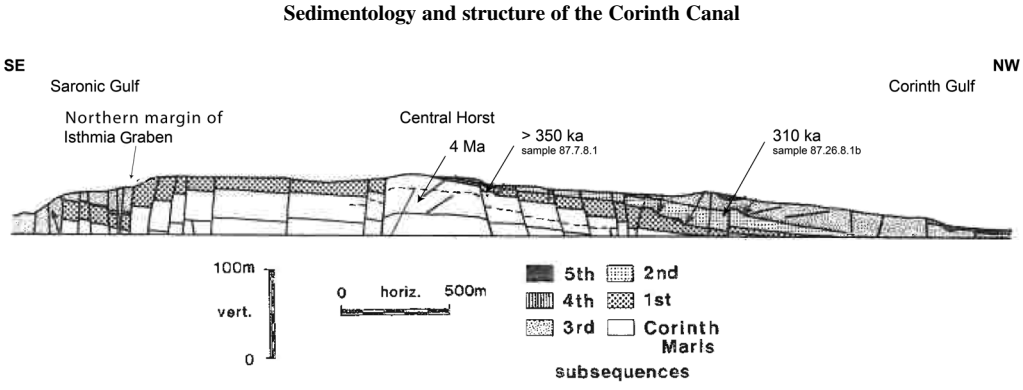

Fig. 2. Modified section of the Corinth Canal proposed by Collier (1990; see fig. 1). This section presents the central horst with the Corinth Marls and the five transgressive subsequences. All the sample numbers refer to the study by Collier (1990). The transcription of the ages from Collier and Dart (1991) is displayed on the section. Corinth Marls are dated at *c.* 4 Ma.

sands that can be associated with a fluvial environment (Papanikolaou *et al.* 2015). In these boreholes, foraminifera assemblages indicate a shallow-marine environment between a lagoon and a more coastal environment at *c.* 175 ka (Papanikolaou *et al.* 2015).

Methods

Fieldwork for this study was conducted from 20 to 27 August 2020; it consisted of sedimentological descriptions and a photogrammetric survey carried out using a drone. Ten high-resolution, millimetre-scale vertical sedimentological sections were described in detail to document the facies (Table 1) and the facies associations (Table 2) along the canal section (see the location in Fig. 1). The sedimentological data included: grain size, grain type, sedimentary structures, colour, texture, and fossil types and bioturbation. Although originally indicated for fluvial deposits, we adopted the Miall facies codes shown in Table 1 (Miall 2006) to describe the textural facies features of the marine deposits. This choice was based on their very similar attributes when compared to fluvial facies.

The drone survey consisted of 24 flights that gave a total of 15 497 photographs to compute the photogrammetric model of the canal, including both of its walls. The model was constructed using Context-Capture from the Bentley suite of software, with the support of F. Poux (University of Liège, Belgium). The model interpretation was performed using IFPEN's Virtuoso software, which enabled work to be carried out on an adaptive zoom mesh model (Schmitz *et al.* 2014). The geometries were constrained and quantified in 3D, sections were then described (Fig. 3). We delimited the sequences based on major unconformity surfaces that are continuous for more than 1 km.

Results

Facies and facies associations

The sediments observed along the Corinth Canal were divided into 21 different facies based on lithology, sedimentary structure, geometry and bioturbation rate. The facies are described in Table 1. The interpretation column in Table 1 proposes the possible depositional processes. The facies are regrouped into eight facies associations (FA) based on their depositional environments and numbered from the base to the top along the vertical section (Table 2).

FA1: Corinth deep-water lacustrine marls (facies Fl). FA1 is mainly composed of laminated carbonate silt with shell debris (facies Fl: Table 1) stacked in a massive 30 m-thick set at the base of the canal section (Figs 4, 5 & 6). The shells were identified by Collier (1990) as freshwater *Viviparus* sp. Plant and wood debris were found in some brownish layers. Moreover, oxidation traces (Fe) associated with bigradational bedding were observed *sensu* Rebesco *et al.* (2014). Beds in FA1 are parallel and continuous at the scale of the canal, up to 1 km long (Fig. 3).

We interpret FA1 as massive settling deposits in a deep-water lake owing to the presence of *Viviparus* sp., in agreement with previous work by Collier (1990) (Table 2). The brownish layers with plant and wood debris are interpreted as fine-grained turbidites, which indicates a continental episodic input that probably took place during a surge potentially transported by hyperpycnal flows (Mulder and Alexander 2001). Finally, the bigradational beds associated with oxidated horizons are interpreted as a reworking by bottom currents (Rebesco *et al.* 2014).

Table 1. *Facies*

Facies	Description	Geometry	Interpretation
Silt			
Fm: massive silt	Massive vertical stacking of carbonate siltstones with horizontal bedding and uneven bed boundaries	Stacking of 0.5 to 2 m	Stacking of settling sediments in deep water (perhaps in an isolated water body)
Fr: bioturbated silt	Bioturbated silt (without soil evidence). The beds are fining-up and thinning-up	Beds are centimetres to decimetres thick. Stacked in units from 0.25 to 1.5 m thick	Stacking of settling sediments in deep water with bioturbation (perhaps in an isolated water body)
Fl: silt with thin laminations	Well-bedded thinly laminated silt beds. Horizontal bedding with: • plant or wood debris in the brownish silt levels; • shells; • debris; • oxidation traces (Fe); • bioturbation; • bigradational bedding. Colour: white to pale grey with a grey patina	Beds are millimetres to centimetres thick with uneven contacts	Fine-grained 'turbidites' with continental input (e.g. surge/hyperpycnal flows) indicated by the presence of wood debris. Reworked by bottom currents; evidence of oxidation traces, bioturbation and bigradational bedding (Rebesco *et al.* 2014)
Fc: silt with gravel lag	White silt with isolated to aligned granules. Granules are matrix supported and mainly aligned. Some bivalve phantoms are observed	Beds are 1–30 cm thick	Settling deposits reworked by bottom currents. The granules are interpreted as lag deposits (Rebesco *et al.* 2014; Rubi *et al.* 2018)
Sand			
Sm: fine- to medium-grained massive sand	Massive to crude inverse- to normal-grading with: • few shells (whole and debris); • bioturbations. Poorly lithified	Beds are 0.5–1.5 m thick	Grain flow (Lowe 1982)
Ssl: very fine- to fine-grained sand with scour and fill	Well-bedded thinly laminated very fine- to fine-grained sand beds with: • gastropods shell debris (gastropods, few bivalves); • vertical bioturbations at the base; • fine-grained ferruginous grains (oxidation traces). Colour: white	Beds are 1–10 cm thick. Uneven contacts. Scour and fill. Undulating scour surface	Scour and fill by a high-velocity flow of water, and filled by very fine- to fine-grained sand that is usually coarse during the waning stage of the flow that cut the scour. The gastropod shells are identified as *Viviparus* sp. and indicate a lacustrine environment (Collier 1990). The bivalve debris is identified as *Cardium* sp. and indicates a marine environment (Collier 1990). The ratio and the conservation between the gastropods shells and bivalve debris indicate a lacustrine environment with a few marine incursions

Sl: well-bedded laminated sands	Well-bedded and laminated very fine-grained sand with: • shells or debris of gastropods and/or bivalves; • a few bioturbations at the base	Beds from 1 to 10 cm thick	Sl facies is interpreted as the deposits of turbiditic flow. The gastropod shells indicate a freshwater environment; the bivalves (*Cardium* sp.) are interpreted as a marine fauna (Collier 1990)
Sp: sand with planar cross-stratification	Medium-grained sandstone with planar cross-stratifications. The alternative direction of the planar oblique stratifications leads to herringbone cross-bedding	Beds are centimetres thick	The planar cross-stratifications indicate a tractive current (Rubin and Carter 1987; Venditti *et al.* 2005). The herringbone cross-bedding highlights a tidal current (James and Dalrymple 2010) with the migration of straight-crested dunes under lower bed-shear-stress values (Rubin and Carter 1987; Venditti *et al.* 2005)
St: sand with trough cross-stratification	Fine- to medium-grained sandstone with trough cross-stratifications	Beds are centimetres thick with large dune geometries	The trough cross-stratifications indicate a tractive current with the migration of sinusoidal-crested dunes under high bed-shear-stress values (Rubin and Carter 1987; Venditti *et al.* 2005)
Sms: bioclastic grainstone	Medium- to coarse-grained sand with shells. Crude grading and bioturbations are observed on top. Poorly lithified	Beds are massive, *c.* 1–1.5 m thick	Foreshore/shoreface deposition of bioclastic grainstone by mainly wave-forced currents (Nemec and Steel 1984; Pemberton *et al.* 2012; Weill *et al.* 2013)
Gr: grainstone with cross-stratification	Bioclastic coarse-grained sand with vertical bioturbations (up to 10 cm)	Beds are centimetres thick. Horizontal and planar cross-stratification	Upper shoreface/foreshore deposition of bioclastic sand by wave-forced currents and/or tidal currents (Nemec and Steel 1984; Pemberton *et al.* 2012; Weill *et al.* 2013)
Conglomerates			
Gmg: conglomerates with mudclasts	Massive, matrix-supported conglomerate with: • clasts: granules to pebbles; • matrix: silt to medium-grained sand; • carbonated erosive base with mudclasts • crude normal grading • bioturbated at the top	Beds are *c.* 1.5 m thick	Subaqueous MTD (Nemec 2009; Nugraha *et al.* 2020)
Floa: floatstone	Massive bed with: • clasts: shell debris (marine) >2 mm and granules; • matrix: micrite • unsorted; • bioturbated at the bottom	Beds are *c.* 0.5–1 m thick	The presence of the floatstone can be explained by the subsequent MTDs. This hypothesis was suggested by Al-Awwad and Pomar (2015), where a MTD can induce the movement of carbonated elements and organisms that can be deposited as a floatstone once the current velocity slows down
Gcm: massive clast-supported granules with pebbles	Massive clast-supported granules and pebbles beds, erosive at the base	Beds are *c.* 1 m thick	High-energy tractive currents (Martín *et al.* 2001, 2009, 2014)

(*Continued*)

Table 1. *Continued.*

Facies	Description	Geometry	Interpretation
Gh: horizontal granules	Horizontal beds of coarse-grained sand to granules with aligned pebbles on the surface. Well sorted and well bedded	Beds are *c.* 10–20 cm thick. Stacked in units 3 m thick	Gravel lag indicates bypass and erosion by high-velocity tractive currents (granules to pebbles) that can be found in strait-centre areas (Longhitano 2013)
Gp : oblique cross-stratified granules	Oblique cross-beds of coarse-grained sand to granules with an aligned pebble level. Well sorted and well bedded	Beds are *c.* 5–20 cm thick. Stacked in units *c.* 1 m thick or in standalone beds	The cross-stratification and the coarser materials indicate the presence of a tractive process (Rubin and Carter 1987; Martín *et al.* 2001, 2009, 2014; Venditti *et al.* 2005)
Gcg: clast-supported granules with normal grading	Stratified clast-supported granules at the bottom to coarse- to very coarse-grained sand at the top. Granules are angular	Beds are 15–25 cm thick and are stacked in units of *c.* 1 m	High-energy tractive current (Martín *et al.* 2001, 2009, 2014)
Gms: bioclastic conglomerate	Bioclastic conglomerate with: • clasts: pebbles, shells and some oysters • matrix: very coarse-grained sand to small granules	Beds are 5–10 cm thick. Units are *c.* 1.5 m thick	Foreshore/shoreface carbonated deposits (Nemec and Steel 1984; Pemberton *et al.* 2012; Weill *et al.* 2013)
RudO: rudstone with oysters	Massive bed with: • clasts: mainly oyster shells and secondary pebbles, shell debris and entire shells; • matrix: micrite	Beds are *c.* 1 m thick	Foreshore framestone or 'Beach rock' (Nemec and Steel 1984; Weill *et al.* 2013)
Soil			
P: carbonated soil	Weathered heterolytic carbonated-rich bed with probable roots	Beds are *c.* 0.5–2 m thick	Soil
Pw: weathered soil	Matrix-supported conglomerate. Pebbles in an unconsolidated reddish matrix	From 0.2 to 2 m-thick units	Soil

Table 2. *Facies associations*

Facies Association	Facies	Units Sequence	Description	Interpretation
FA1 Corinth deep-water lacustrine marls	Fl	Unit 1 Sequence 1	Laminated carbonate silt with shell debris (Fl) stacked in a massive 30 m-thick set with plant and wood debris and *Viviparus* sp. (Collier 1990)	Massive settling deposits in a deep-water lake due to the presence of *Viviparus* sp., in agreement with the previous work of Collier (1990), and with continental episodic surge potentially transported as hyperpycnal flows (Mulder and Alexander 2001)
FA2 Lacustrine to marine marls	Fl, Ssl, Fm and Gh	Units 2, 3, 4 and 5 Sequence 1	Laminated silt (Fl) with small-scale truncations produced by scour and fill of very fine- to fine-grained sand (Ssl), and massive silt (Fm) and gravel lag (Gh)	Episodic marine transgressions (Ssl, *Cardium* sp.) in a lake environment (Fl, *Viviparus* sp.)
FA3 Sand-rich brackish deposits	Fr, Sm, Sl, Fc, Fl and Gh	Unit 6 Sequence 1	Massive sand units (Sm), gastropod- and bivalve-rich sand (Sl), laminated and/or bioturbated silt deposits (Fl and Fr) and granules lags (Gh)	Brackish environment indicated by the mix between lacustrine (*Viviparus* sp.) and marine species bivalves (*Cardium* sp., Collier 1990).
FA4 Mass Transport Deposits	Gmg, Floa and Gh	Unit 7 Sequence 2	MTD (Gmg) associated with floatstone (facies Floa)	Debris flow is probably induced by seismic activities from the margins of the basin
FA5 Soil	P and Pw	Unit 8 Sequence 2	Soil formation with roots (P) and alteration of the carbonate-rich facies by weathering (Pw)	Palaeosol (Collier 1990)
FA6 Conglomerate tidal dune strait	Gp, St, Sp, Gh, Gmg, Fc, Sm and Gcm	Units 9, 10 and 11 Sequence 3	Planar and trough cross-stratified sands, granules and conglomerates interbedded with herringbone cross-bedding showing two opposite downlapping directions towards the NW and the SE ranging from facies scale to large scale	Erosion on the central horst with bedload parting (i.e. zone 'A', strait-centre zone), which form the sill of the strait Conglomerate tidal dune-bedded strait zone (i.e. zone 'B') mainly characterized by the large-scale dunes and herringbone cross-bedding
FA7 Upper shoreface to beach foreshore	Gr, RudO, Gms and Gmg	Unit 12 Sequence 4	Coarsening-up thick units of bioclastic grainstones (Gr) rudstones that contain oysters (RudO), bioclastic conglomerates (Gms) and MTDs (Gmg) with internal cross-stratification, and with oyster shells and a few pebbles	The rudstones, bioclastic grainstones and conglomerates are interpreted as an upper shoreface to beach foreshore facies association in a marine environment
FA8 Continental environment	Gmg and Gh	Unit 13 Sequence 4	Horizontal granule beds (Gh) interbedded with massive metre-thick MTD conglomerates (Gmg)	Continental environment deposit with alternating MTDs and transient stream deposits, probably with a distal alluvial fan near the shoreline

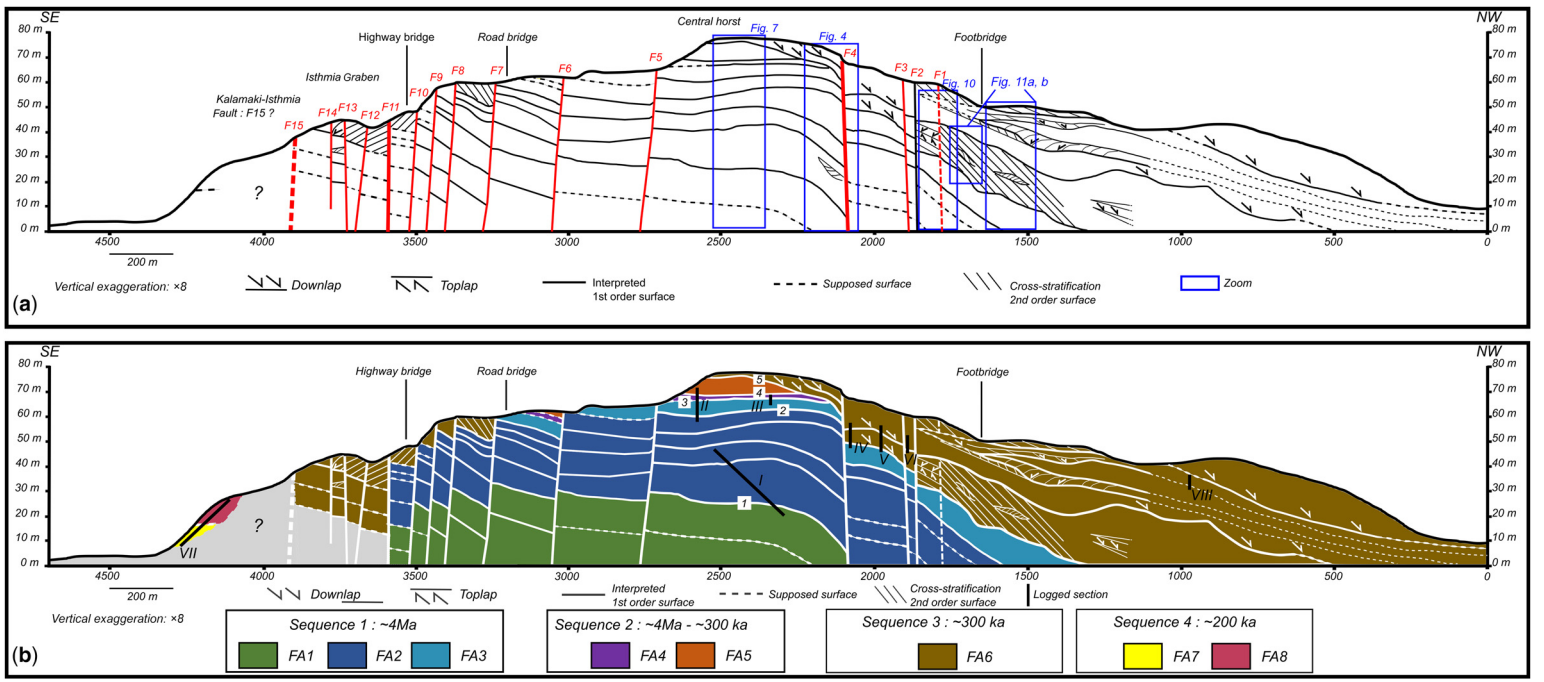

Fig. 3. Sections of the SW wall of the Corinth Canal. (**a**) Structural section displaying all of the features identified in the field or the model. The faults are numbered from NW to SE, and the location of the Isthmia Graben and the horst are based on the section by Collier (1990, fig. 2). (**b**) Section showing the facies associations (FAs), the logged sections and identification of the numbered unconformity surfaces that define the sequences associated with their age, based on Collier (1990) and Collier and Dart (1991).

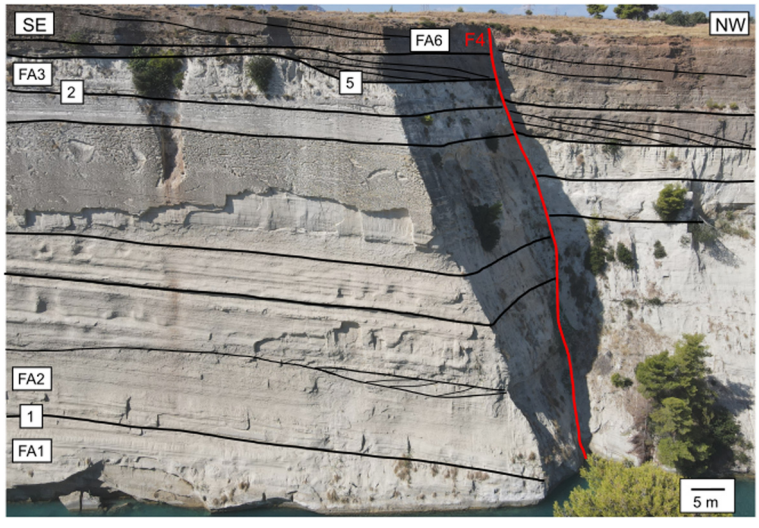

Fig. 4. Close-up of the structures located in Figure 3. In FA2, some hummocky cross-stratification at a large scale is observed. In FA6, the cross-stratification and the laminations are orientated towards the NW. The numbers represent the FA limits and the red line a fault (here F4).

FA2: lacustrine to marine marls (facies Fl, Ssl, Fm and Gh). FA2 crops out in the central part of the canal section over a length of 2 km and with a thickness of 30 m (Figs 3 & 4). Some scour-and-fill and undulating scour surfaces cut into planar horizontal to low-angle bedding, both at the outcrop scale (i.e. in a logged section: Fig. 5) and at larger scales (Fig. 4). FA2 is mainly composed of laminated silt (facies Fl: Table 1; Fig. 6) and shows small-scale truncations produced by scour and fill of very fine- to fine-grained sand (facies Ssl: Table 1; Figs 5 & 6). Moreover, gravel lag (facies Gh: Table 1; Fig. 6) and massive silt (facies Fm: Table 1; Fig. 6) complete the FA2. The proportion of *Viviparus* sp. (Collier 1990) increases from base to top.

The presence of *Viviparus* sp. indicates a freshwater environment (Collier 1990). The scour-and-fill fine-grained sandstones (facies Ssl) also contained bivalve debris that were identified as *Cardium* sp. by Collier (1990) and which indicate a marine environment. This Ssl facies may indicate episodic marine transgressions (*Cardium* sp.) in a lake environment (facies Fl: *Viviparus* sp.). In summary, FA2 is assumed to have been deposited in an isolated lake with episodic marine connections.

FA3: sand-rich brackish deposits (facies Fr, Sm, Sl, Fc, Fl and Gh). FA3 is a sand-rich facies association (facies Sl and Sm: Table 1; Fig. 6) that is characterized by massive sand beds (facies Sm), gastropod- and bivalve-rich sand (facies Sl), laminated and/or bioturbated silt deposits (facies Fl and Fr: Table 1; Fig. 6), and granules lags (facies Gh). The FA3 thickness ranges between 5 and 10 m (Figs 3, 4 & 7). Some sand beds are very rich in *Viviparus* sp. and other are composed of bivalve shells (*Cardium* sp.), whole or in debris (Sl). The silt associated with the granule lags (facies Fc, Fl and Gh) does not present shells of any kind. The base of FA3 could have been subjected to erosive events associated with some granule lags (facies Gh: Fig. 8).

We interpret the sand-rich FA3 as a brackish environment, as indicated by the mix between lacustrine (*Viviparus* sp.) and marine species (bivalves: Collier 1990). Indeed, the higher concentration of bivalves in comparison to gastropods indicates a transition from a lacustrine environment to a marine environment. Moreover, the gravel lags (facies Gh), laminated sands (facies Sl) and silts (facies Fl) without shells are interpreted as having come from the shore into a high-energy current environment.

FA4: mass transport deposits (facies Gmg, Floa and Gh). FA4 is dominated by mass transport deposits (MTDs) (facies Gmg: Table 1; Fig. 9) associated with floatstone (facies Floa: Table 1; Fig. 9). The MTDs (facies Gmg and Floa) are erosive at the base and eroded at the top (Fig. 7). The beds are between 1 and 1.5 m thick (Figs 7 & 8). FA4 is 1–3 m thick and is only found along a length of *c.* 700 m in the central part of the canal section (Figs 3 & 7).

We interpret FA4 as a debris flow without interbedded tidal deposits. This debris flow was probably derived from the collapse of portions of cliff margins caused by seismic activity.

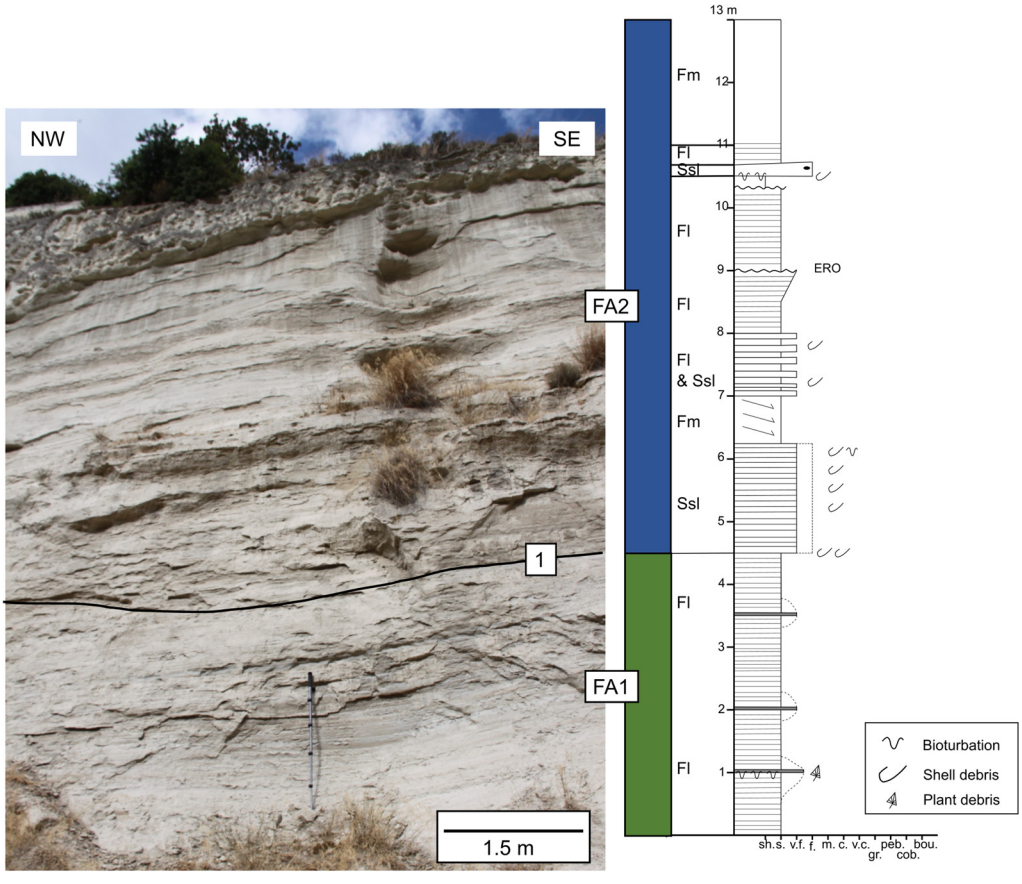

Fig. 5. Outcrop of the logged section displaying FA1 and FA2. The logged section is located in Figure 3 (I in Fig. 3b). The numbered surface represents the first unconformity surface.

FA5: Soil (facies P and Pw). FA5 consists of a soil with roots (facies P: Table 1; Fig. 9) and weathered carbonate-rich sediments (facies Pw: Table 1). The thickness of FA5 varies from 0.5 to 10 m and crops out along 700 m in the central part of the canal section (Figs 3 & 7). We agree with Collier (1990), who identified this FA as a soil with local karstifications.

FA6: strait conglomerate tidal dunes (facies Gp, St, Sp, Gh, Gmg, Fc, Sm and Gcm). FA6 consists mainly of planar and trough cross-stratified sands, granules and conglomerates interbedded with herringbone cross-bedding in a partially reddish matrix (Fig. 10). FA6 is thicker on both ends of the canal section (20 m thick in the SE and 40 m thick in the NW) and eroded or undeposited in its central part (Figs 3, 4, 7, 10 & 11). The base of FA6 is erosive, and the first-order surfaces are erosive, as evidenced by both toplap and downlap stratal terminations and undulated surfaces (Figs 3, 4, 10 & 11). The planar and trough cross-stratifications that downlap in two opposite directions (NW and SE) are delimited by the F10 fault: they dip towards the NW to the NW of the F10 fault, and towards the SE to the SE of the F10 fault (Fig. 3).

On the NW end of the canal section, we observed second-order surfaces that consist of large-scale asymmetrical herringbone cross-bedding with lower and thicker (*c.* 7 m) foreset bedding with a low angle (*c.* 10°) to the NW, and upper thinner (*c.* 1.5 m) foreset bedding with a higher angle (20°) to the SE (Fig. 10). At the third order, we document compound-dune formations with dominant foreset deposition towards the NW and a subordinate reverse foreset direction towards the SE (Fig. 11).

At the facies scale, FA6 is dominated by oblique cross-stratified conglomerates (facies Gp), and trough (facies St) and planar (facies Sp) oblique cross-stratified sandstones (Table 1; Figs 12, 13 &

Fig. 6. Photographs of facies FA1, FA2 and FA3; the facies descriptions are given in Table 1.

14). These oblique cross-stratified deposits can be overlain by horizontal clast-supported conglomerates (facies Gh, Gcg and Gcm), gravel lags (facies Fc) and massive sandstones (facies Sm: Table 1; Figs 12, 13 & 14). The oblique cross-stratification (facies Gp, St and Sp) is outlined by metre-thick beds internally organized into centimetre- to decimetre-thick foresets based on erosional surface, and are normally graded (Figs 12 & 13); the tops of the beds can be either eroded or preserved (Fig. 12). The facies grain-size sorting shows a high variability from very poorly sorted to well-sorted clasts (Fig. 13a, b). We report occurrences of herringbone cross-bedding in medium-grained sandstones (facies Sp) interbedded with horizontal conglomerates (facies Gh: Fig. 13c). Along the logged section, no evidence of mud is observed.

Based on the criteria proposed by Longhitano and Chiarella (2020), we interpret FA6 as a sandy-conglomeratic tidal dune complex accumulated in a strait. Evidence for this interpretation includes planar and trough cross-stratification of sands, granules and conglomerates showing two opposite downlapping directions towards the NW and SE that vary from facies to large scale. In consequence, at both ends of the central horst FA6 dips preferentially in two main opposite directions away from the central high. Based on the last generalized model for tidal straits proposed by Longhitano and Chiarella (2020), we interpret the horst as the location of a bed-load parting (i.e. zone 'A', strait-centre zone) that forms the constriction and the sill here of the strait. In this area, sediments produced by erosion and bypass were transported outwards to both the SE and NW strait exits, and formed the dune-bedded strait zone (i.e. zone 'B') that is mainly characterized by large-scale cross-bedding (Longhitano and Chiarella 2020). A complementary interpretation is proposed by Dalrymple (2022): the two oppositely directed cross-bedded deposits could represent the

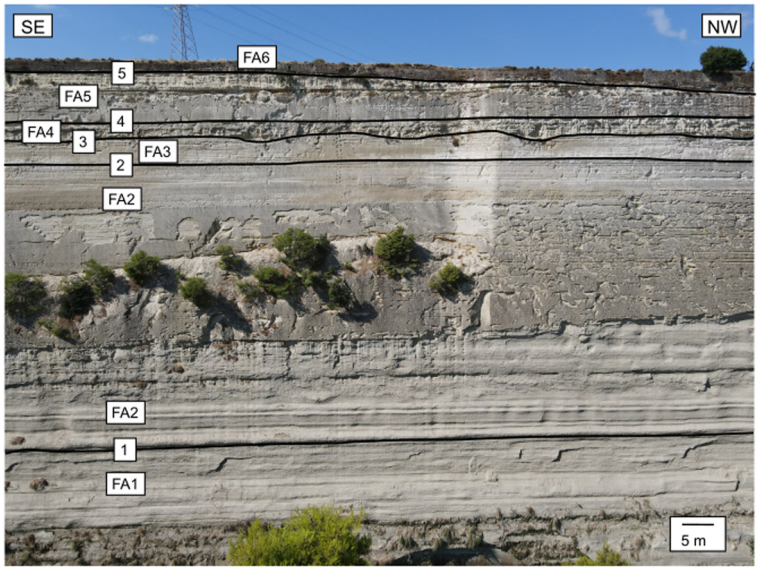

Fig. 7. Close-up on the area in Figure 3b displaying all of the facies associations (FAs) cropping out in the central horst block. Numbers 1–5 refer to the boundaries between the FAs.

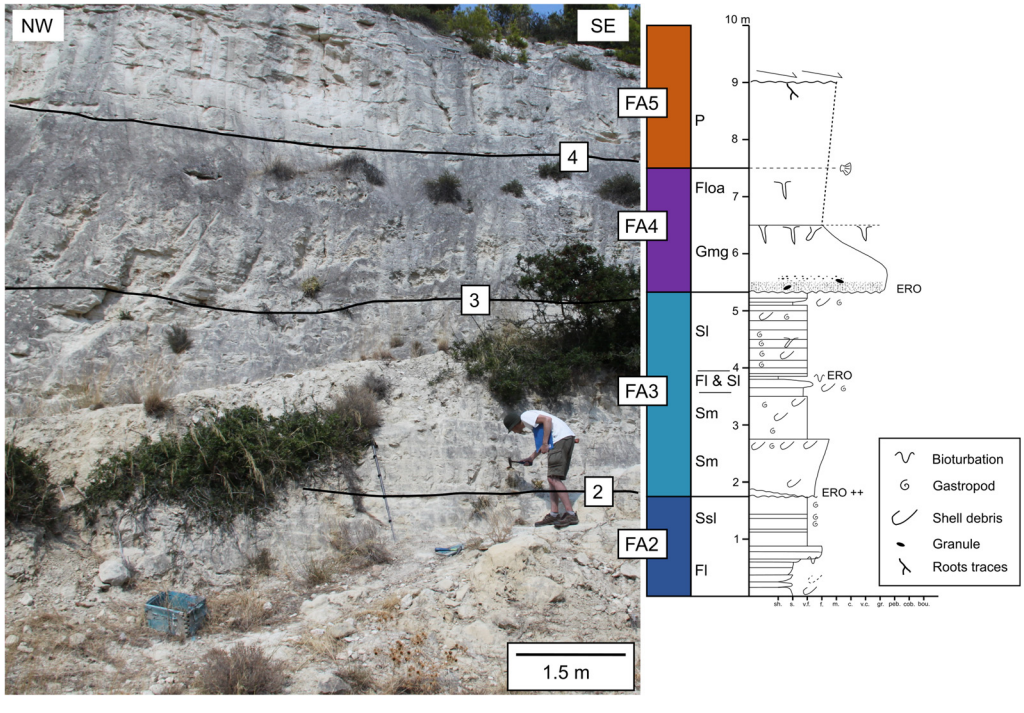

Fig. 8. Outcrop of the logged section displaying FA2, FA3, FA4 and FA5. The logged section is located in Figure 3 (II in Fig. 3b). The numbered surfaces represent the second, third and fourth unconformity surfaces, respectively.

Fig. 9. Photographs of facies FA4 and FA5; the facies descriptions are given in Table 1.

two 'constriction-related deltas' (CRDs) that develop in the strait areas of flow expansion as the sediment is transported away from the bedload parting/constriction.

Moreover, the tabular cross-stratification is interpreted as having formed by migration of straight-crested dunes under lower bed-shear-stress values (facies Sp: Table 1) (Costello and Southard 1981; Harms *et al.* 1982; Rubin and Carter 1987; Ashley 1990; Venditti *et al.* 2005). The trough cross-stratification reflects the migration of sinusoidal-crested dunes under high bed-shear-stress values (facies St: Table 1) (Rubin and Carter 1987; Venditti *et al.* 2005). To create such dune-bedded structures, the depositional current velocity is estimated to range from 1 to 2 m s^{-1} (Ashley 1990; Stow *et al.* 2009; James and Dalrymple 2010).

Second, we identified herringbone cross-stratification with a strong asymmetry. The NW-dipping foresets are thicker with a lower angle than the SE reverse foresets. We interpret this structure to be the result of asymmetrical tidal currents with a dominant flow towards the NW and a reverse secondary flow towards the SE (Dalrymple *et al.* 1992; James and Dalrymple 2010). Asymmetrical tidal currents are preferentially reported in straits due to the cyclical amplification of one tidal phase over the opposite phase induced by passage through the central constriction (Reynaud and Dalrymple 2012; Longhitano 2013).

Third, the mud-free facies association (FA6) is another criterion used to recognize a dune-bedded strait from other tidal environments due to its high-energy setting (Longhitano and Nemec 2005). The mud paucity in tidal systems can also be due to their distance from a source of mud (James and Dalrymple 2010). Here, the sediment sources are very close to the canal; in particular the Perachora horst to the north, which is made up of ophiolitic rocks. Hence, the lack of mud in FA6 is probably due to

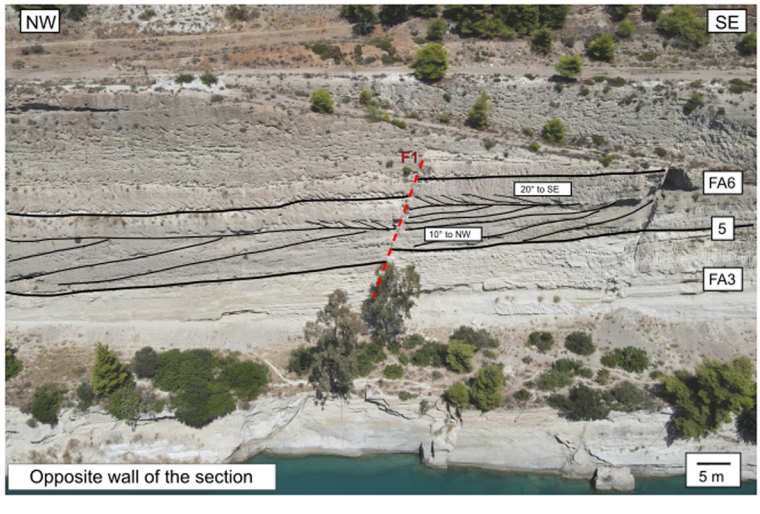

Fig. 10. Close-up of the asymmetrical herringbone cross-stratification with the main migration direction towards the NW (FA6). The thicker lines represent the first-order surfaces, the medium lines represent the second-order surfaces and the thinner lines are the third-order surfaces.

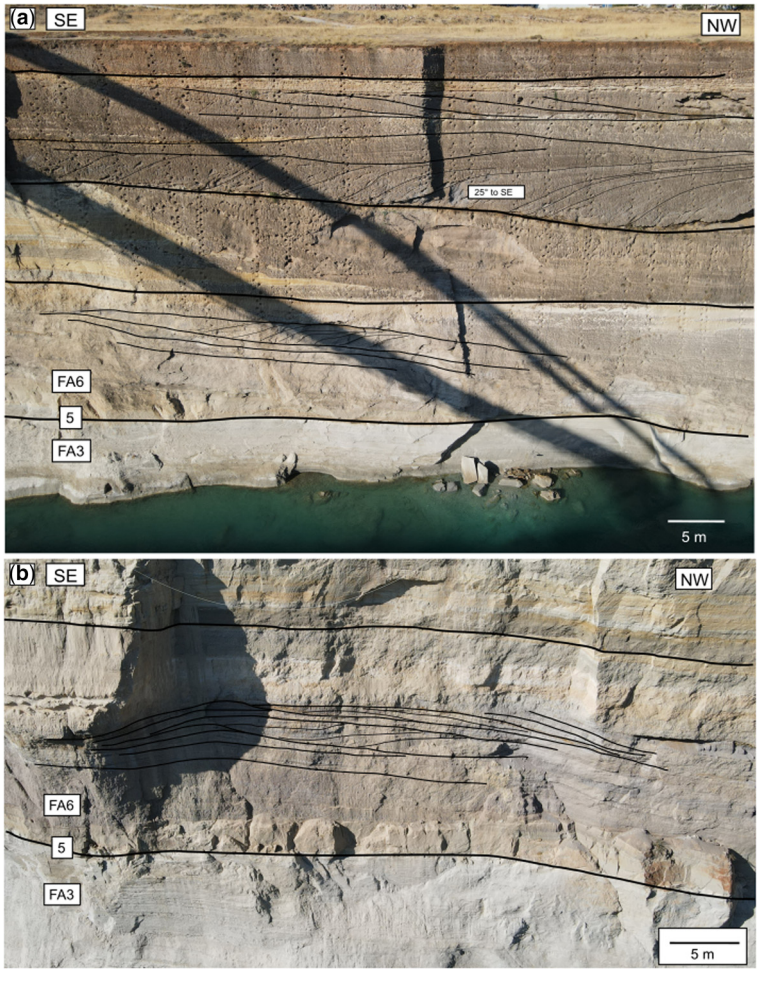

Fig. 11. Close-up of some of the compound-dune features cropping out in the FA6 conglomeratic beds with the migration direction towards the NW and the secondary reverse foreset direction towards the SE. (**a**) Second-order surfaces (medium thickness lines) are observed to be downlapping onto first-order surfaces (thickest lines; to the NW). The third-order surfaces (thinner lines) downlap in the opposite direction (to SE) on both the first- and second-order surfaces, forming dune structures. The dip angle is larger for the surfaces downlapping towards the SE than for the surface downlapping to the NW. (**b**) Similar features to those shown in (a).

energetic tidal currents transporting mud in suspension away from this depositional area of the strait.

Fourth, compared to other tidal environments, the thickness of FA6 (at least 40 m thick) also argues for a tidal strait environment (Longhitano and Chiarella 2020).

Fifth, we observe compound foreset architectures (Fig. 11), which are interpreted as dunes derived from the superimposition of smaller simple dunes on top of large dunes by tidal reverse flows. These dune architectures are reported in inshore tidal environments, as well as in tidal estuaries, tidal deltas and tidal straits (Dalrymple *et al.* 1992, 2012; Longhitano and Chiarella 2020). In micro-tidal settings, such as in the Mediterranean Sea, tidal deltas and tidal estuaries are unusual depositional systems (Longhitano and Colella 2007) and are probably not strong enough to generate large-scale coarse-grained dunes. However, tidal dunes of medium- to coarse-grained sand up to gravel, which can be up to 10 m in height, are documented in the centre of the Messina Strait (Barrier 1984; Montenat *et al.* 1987; Longhitano 2018*a*) with associated current velocities that vary between 1 and 3 m s^{-1} (Santoro *et al.* 2002).

FA7: upper shoreface to foreshore (facies Gr, RudO, Gms and Gmg). FA7 is a *c.* 15 m-thick

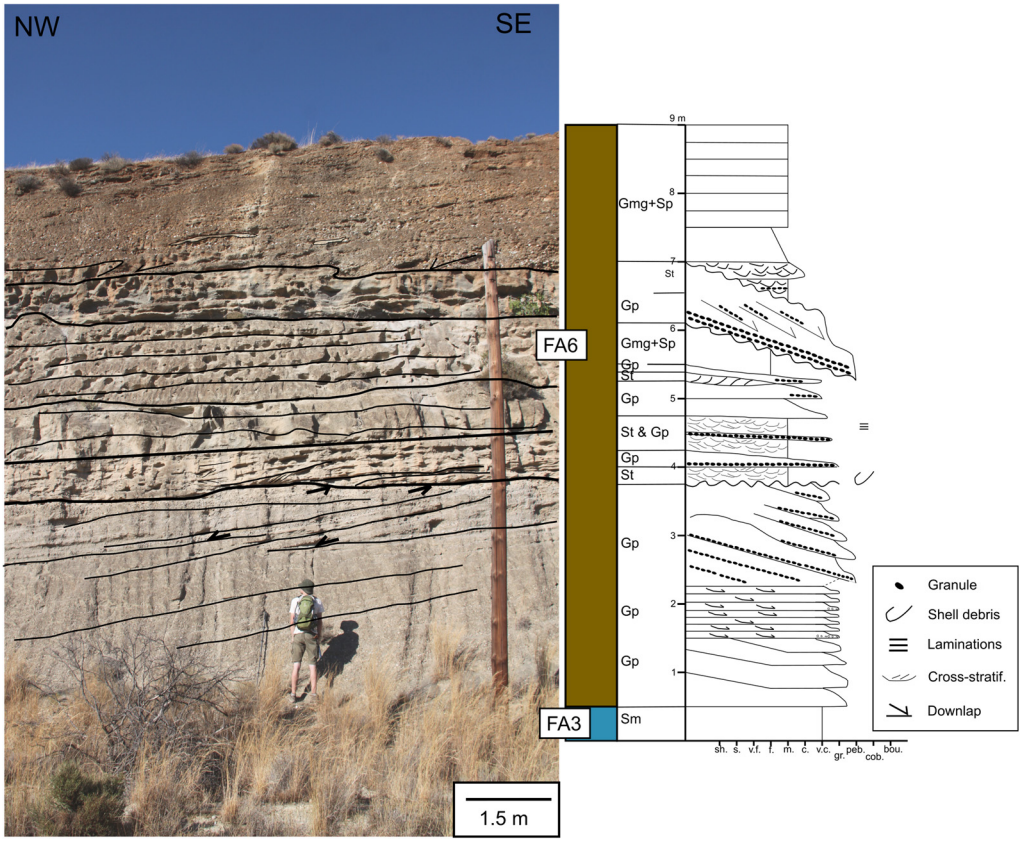

Fig. 12. Outcrop and sedimentological logged section of FA6. The logged section is located in Figure 3 (V in Fig. 3b).

coarsening-up set of bioclastic grainstones (facies Gr: Table 1; Figs 15 & 16), rudstones that contains oysters (facies RudO: Table 1; Figs 15 & 16), bioclastic conglomerates (facies Gms: Table 1; Figs 15 & 16) and small-scale MTDs (facies Gmg: Table 1; Figs 9 & 15). The grainstones (facies Gr) are thinly laminated (centimetre-thick beds) and stack in massive metre-thick strata with internal cross-stratification (Fig. 15). The rudstones consist of metre-thick beds that contain oyster shells and rare pebbles (Fig. 15).

The rudstones, bioclastic grainstones and conglomerates are interpreted as an upper shoreface to foreshore facies association in a marginal-marine environment (Pemberton *et al.* 2012; Isla *et al.* 2020).

FA8: alluvial fan (facies Gmg and Gh). FA8 is a *c.* 5 m-thick set of decimetre-thick horizontal granule beds (facies Gh: Table 1; Figs 6 & 15) interbedded with massive metre-thick MTD conglomerates (facies Gmg: Table 1; Figs 9 & 15). The horizontal granule beds are clast-supported and display internal pebble lag surfaces (Fig. 15). We interpret FA8 as an alluvial fan deposit with alternation between MTDs (facies Gmg) and transient stream deposits (facies Gh). The facies are sometimes consolidated with a carbonate-rich matrix that may be the result of an early marine diagenesis. FA8 is dominated by a large sediment supply that formed an alluvial fan probably close to a coastal environment.

Fault evolution

We measured fault directions and dips in the field and with the 3D model (Fig. 3). The faults were numbered from NW to SE. Their characteristics are reported in Table 3. Both north- and south-dipping normal faults share a mean strike direction N74, which corresponds to the N160 extension of the Eastern Corinth Rift (Armijo *et al.* 1996; Moretti *et al.* 2003). The north- and south-dipping normal faults caused the formation of the central horst (Collier 1990) (Figs 2 & 3). Their architecture (Fig. 3) allows the syntectonic sequences to be identified.

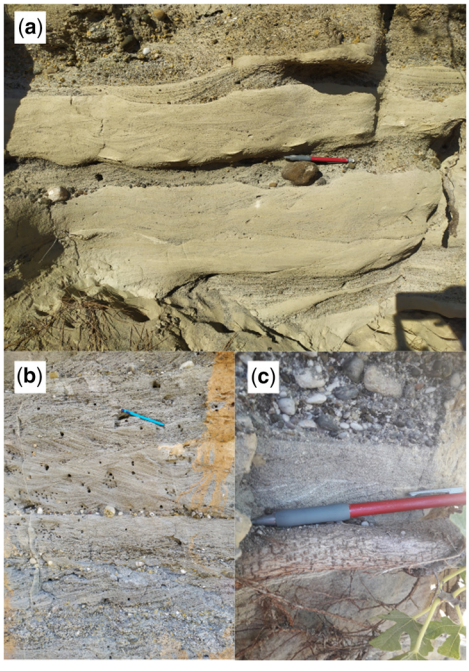

Fig. 13. FA6 facies variability. (**a**) Variability in the St facies from very poorly sorted with heterogeneous granulometry to well sorted with similar granulometry. (**b**) Variability in the St facies with more granular elements. (**c**) Herringbone cross-bedding in the Sp facies.

Two tectonic pulses can be highlighted (Fig. 17). The first pulse occurred after deposition of Sequence 2 with continuous activity during the deposition of Sequence 3 in the central part with faults F2, F4 and F6–F11. This first pulse resulted in the uplift of the central horst, which was bounded by north- and south-dipping normal faults. This horst, located between the Corinth Gulf and the Aegean Sea, could produce a sill depending on the sea level and the horst elevation. The second pulse after Sequence 3 was associated with the activity of the major Kalamaki–Isthmia Fault (F15) and associated minor faults F12–F14. The Kalamaki–Isthmia Fault accommodated the uplift of the Isthmus of Corinth as opposed to the subsiding eastern Aegean area. This last fault activity (F15) was estimated to have occurred at 175 ka in the area (Papanikolaou *et al.* 2015). In summary, the fault activities document a migration of the extension from the NW to the SE.

Tectonosedimentary evolution

Traditional sequence stratigraphy, based on simple shelf/delta architecture with a constant subsidence rate, is difficult to apply to tectonically active tidal straits. We thus based the tectonosedimentary evolution on the facies associations and their relative depositional environments in order to constrain the palaeobathymetries and palaeoenvironments (i.e. lacustrine or marine settings). We integrated our sedimentological observations and fault analyses with

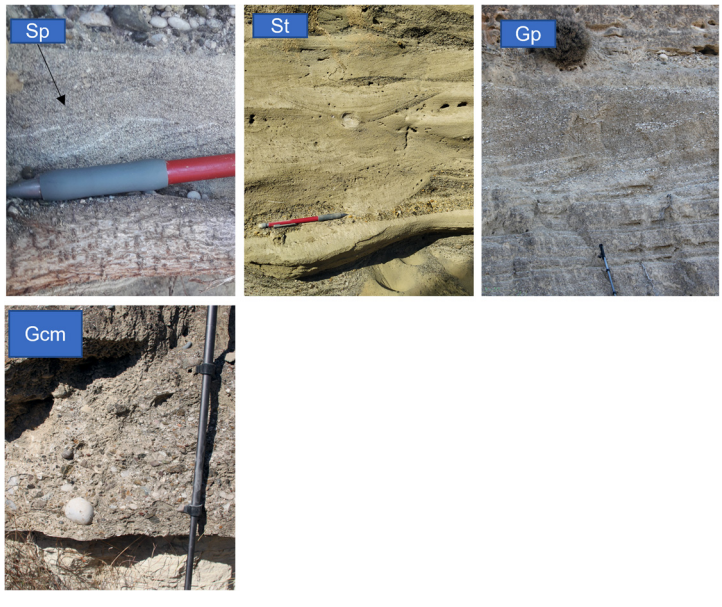

Fig. 14. Photographs of facies FA6; the facies description is given in Table 1.

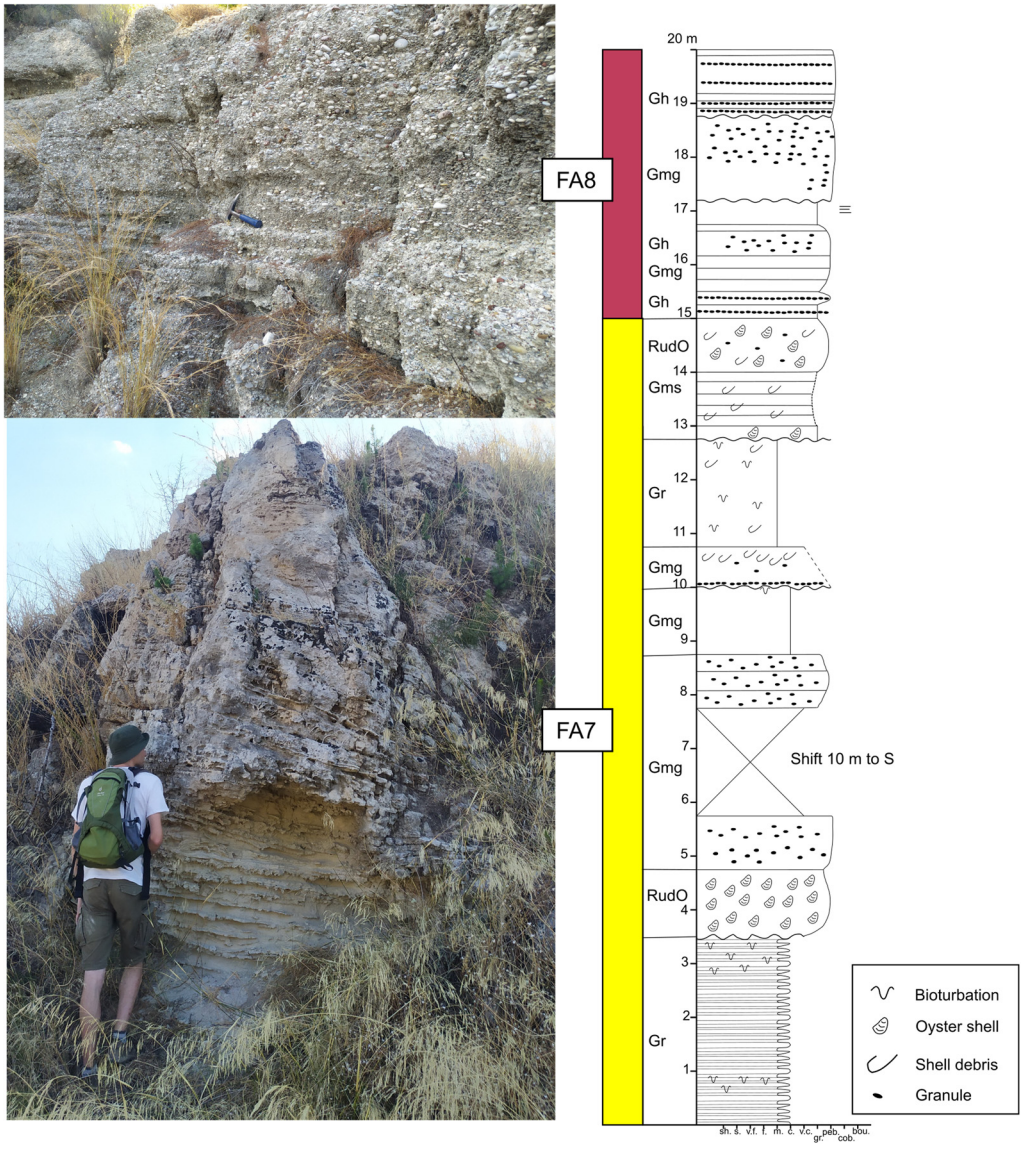

Fig. 15. Outcrop and sedimentological section of FA7 and FA8. The logged section is located in Figure 3 (VII in Fig. 3b).

previous dates given by Collier (1990), Collier and Dart (1991) and Collier and Thompson (1991) with the Corinth Rift regional evolution (Ori 1989; Taylor *et al.* 2011; Ford *et al.* 2013; Nixon *et al.* 2016; Rohais and Moretti 2017; Gawthorpe *et al.* 2018; McNeill *et al.* 2019) and with the constraints of marine terraces (de Gelder *et al.* 2019).

Sequence 1. We identified a first sequence (Figs 3 & 17) with a progressive transgression from the deep lacustrine FA1 (Corinth deep-water lacustrine marls) to the lacustrine with marine incursion FA2, and then to the shallow brackish FA3. FA2 and FA3 constitute a transgressive system track. The change from lacustrine to marine and brackish conditions is due to the opening of a connection between the formerly isolated 'Corinth Lake' and the larger Mediterranean Sea. This opening must have been induced by local subsidence of the connecting area due to normal faulting, and not by regional subsidence. Indeed, the connection resulted in a global diminution of the basin bathymetry and the observed

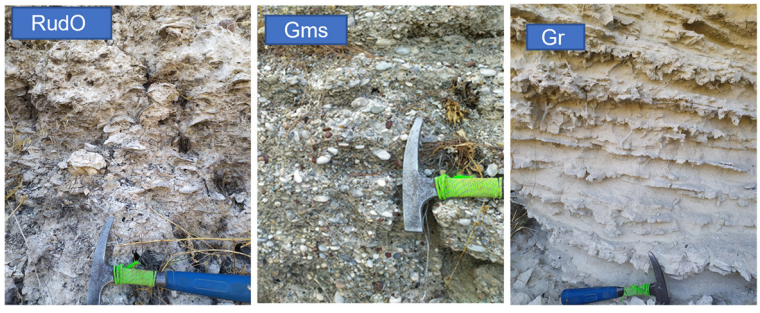

Fig. 16. Photographs of facies FA7 and FA8; the facies descriptions are given in Table 1.

change from a deep (FA1) to a shallow basin (FA3: Figs 3, 4 & 5). The Corinth Marls in FA1 have been dated to *c.* 4 Ma using intrusive magmatic dykes (Fig. 1) (Collier and Dart 1991).

Sequence 2. The unconformity surface 3 lies above the first sequence and corresponds to the top of FA3 (Fig. 3). This unconformity is overlain by a MTD (FA4) and palaeosol deposits (FA5). FA4 and FA5 form the second sequence, which is thin with a maximum thickness of less than 18 m. Sequence 2 is deeply eroded by the unconformity surface 5. This erosion affects Sequence 1 and Sequence 2 from FA2 (Fig. 3). The thin and discontinuous Sequence 2 is located between two major unconformities (surfaces 3 and 5: Fig. 3).

Sequence 3. Above unconformity 5, we observe FA6 downlapping onto it in opposite directions on each end of the horst: that is, SE downlapping on the SE end of the horst and NW downlapping on its NW end. We interpret this unconformity (surface 5) as a transgression from a continental area (Sequence 2, FA5) to a tidal strait (Sequence 3, FA6) that connects the Corinth Gulf with the Aegean Sea (Fig. 3).

Thanks to the U/Th dating provided by Collier (1990), we were able to tie FA6 to MIS (Marine Isotope Stage) 9–MIS 8 (337–300 ka). These deposits are the last evidence of a marine connection between the Corinth Gulf and the Aegean Sea in the canal area. Due to the uplift and the activity of the eastern faults F11–F15 (i.e. the Kalamaki–Isthmia normal fault system), the Isthmia Graben was progressively disconnected from the Aegean Sea.

Sequence 4. Sequence 4, represented by FA7 and FA8, is limited to the hanging wall of the major

Table 3. *Normal faults of the canal section*

Name	Direction (°E)	Dip (°) and direction of dip	Offset (m)
F1	68.9	67.6 N	*c.* 5
F2	85.1	88.9 N	*c.* 7
F3	85.6	85.1 N	*c.* 7
F4	84.3	60.8 N	*c.*13
F5	62.6	65.5 S	*c.* 3
F6	90.3	80.2 S	*c.* 8
F7	85.0	77.3 S	*c.* 11
F8	77.6	76.5 S	*c.* 11
F9	72.4	78.6 S	*c.* 7
F10	73.3	76.7 S	*c.* 7 (estimated)
F11	62.3	72.2 S	Major displacement (20 m minimum, supposed)
F12	75.2	74.7 S	*c.* 5 (estimated)
F13	64.7	68.9 N	*c.* 2 (estimated)
F14	57.5	74.0 N	*c.* 2 (estimated)
F15	*c.* 65	South	*c.* 150 (Pallikarakis *et al.* 2018)
Kalamaki–Isthmia normal fault (Papanikolaou *et al.* 2015; Pallikarakis *et al.* 2018)			

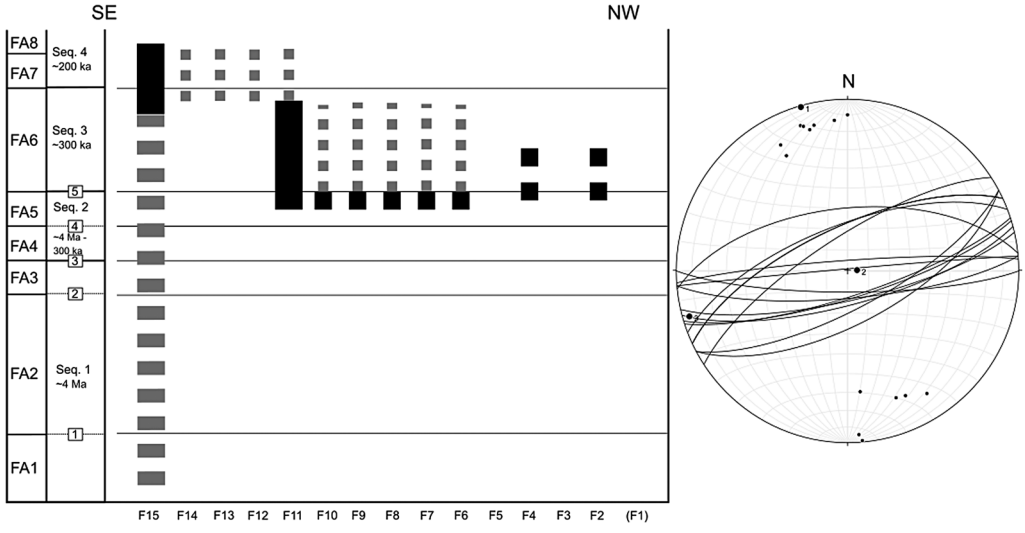

Fig. 17. Schematic chronology of fault appearance and activity. The width of the lines indicates the importance of the fault. The grey dashed lines represent supposed activity. The fault directions are displayed on the stereonet.

Kalamaki–Isthmia normal fault (F15). FA7 documents a foreshore to shoreface environment and is thus interpreted as a highstand deposit dated at 205 ka: that is, MIS 6 as determined by Collier (1990) and confirmed by Pallikarakis *et al.* (2018).

Discussion

Strait-centre zone

An important finding is that the Corinth Strait was active during major fault activity affecting the study area. Indeed, the faulting in this area post-dates Sequence 2 deposition, implying that the faulting is syn- to post-Sequence 3 (*c.* 300 ka). This observation may support the hypothesis that the Corinth Strait was controlled by normal faults (F4 and F5–F7: Figs 3 & 17). The central horst forms the sill and strait-centre zone (i. e. zone 'A': Longhitano 2013; Longhitano and Chiarella 2020); and the hanging walls on both sides correspond to the intermediate tidal strait depositional areas where accommodation enhanced deposition and sediment preservation.

Generally, strait-centre zones are dominated by erosion and the bypass of sediments, and can be considered as a bedload parting area formed under the strongest currents that are amplified by the strait constriction (Longhitano and Chiarella 2020 and references within). Consequently, only coarse-grain deposits may form gravel-size materials, building patches and ribbons that form 10–20 m-wide and 4–5 m-deep lenses. In tectonic horsts, these deposits are organized into sedimentary wedges on each flank of the horst (Longhitano and Chiarella 2020). Moreover, large-scale dunes, up to 10 m high, composed of medium- to coarse-grained sand or even gravel are also documented in tidal strait centres (Barrier 1984; Montenat *et al.* 1987; Longhitano 2018*a*, *b*).

However, in our study area, any coarse-grained deposits crop out in the strait-centre zone. Indeed, the strait-centre zone is made up of fine-grained sediments: a palaeosoil (FA5), MTDs (FA4) and sand-rich brackish deposits (FA3). These deposits are assumed to be older and so are considered pre-strait. In Figure 3, surface 5 shows a lower erosion rate than on its sides, evidencing a bypass without any deposition.

Dune-bedded strait zones: a coarse-grained example

Our FA6 interpretation is based on observations of sandy-conglomeratic dunes with simple and compound foreset architectures. Moreover, the herringbone cross-stratification shows a strong asymmetry with the thicker NW-dipping foresets and their lower angle than the SE reverse foresets. We argue that these sedimentary structures reflect tidal conditions (Pugh 1987; Greb and Archer 1995; Longhitano and Chiarella 2020) and not longshore currents (Collier 1990). The dune long axis is orientated NE–SW, and the dunes show a main forward accretion towards the NW on the NW end of the horst/strait and towards the SE on the opposite end. These orientations and forward accretion are consistent with tidal dune formation under NW–SE-flowing tidal currents (Olariu *et al.* 2012) and

are consistent with the NW–SE orientation of the gateway. We support the previous, if not the first, interpretation made by von Freyberg (1973) that this dune-bedded complex (FA6 in our study) was built in a tidal environment. The NE–SW-orientated dunes of FA6 that were deposited on each side of the horst with opposing dips form the dune-bedded strait zones (zone 'B' in Longhitano and Chiarella 2020).

In dune-bedded strait zones, the existing depositional model is dominated by, if not exclusively formed by, sand dune-bedded facies with 3D and 2D tidal dune fields (Barnard *et al.* 2006; Ferranti *et al.* 2008; Lamarche *et al.* 2011; Longhitano 2011, 2013, 2018*a*, *b*; Longhitano and Steel 2016; Longhitano and Chiarella 2020). Based on Dalrymple and Rhodes (1995), the associated bathymetric depths range from *c.* 20 to 80 m for sand dunes 5–10 m in height. We propose to complete the existing tidal strait depositional model with conglomerate tidal dune deposits. In consequence, the conglomerates are not restricted to MTDs in the tidal strait margin, or to patches and ribbons in the strait centre (Longhitano 2013; Rossi *et al.* 2017; Longhitano and Chiarella 2020), or in strait beaches and shorefaces (Frey and Dashtgard 2011) but can create thick sets of conglomerates that form tidal dune complexes in the intermediate strait areas.

The clasts in the tidal dunes are mainly composed of ultrabasic rocks that were derived from a source to the north where an ophiolitic thrust sheet is present (Fig. 1) (von Freyberg 1973; Collier 1990). The length of the central horst (*c.* 1 km) that forms the strait-centre zone and its fine-grained facies do not enable it to feed the sedimentary volume of FA6. In consequence, we propose that the conglomeratic sediments were mostly supplied from the north probably by a Gilbert-type delta that could provide unconsolidated conglomerates from the foreset to the bottomset (Poulimenos *et al.* 1993; Malartre *et al.* 2004; Rohais *et al.* 2008; Ford *et al.* 2009, 2013; Rubi *et al.* 2018) rather than from the erosion of the central horst. Therefore, it can thus be suggested that in high conglomerate-sediment-supply settings, such as in the Corinth Rift, the depositional tidal strait system led to the formation of conglomeratic tidal dunes on both sides of the strait. Further research should be undertaken to investigate the lateral and vertical evolutions of this kind of coarse-grained system.

Corinth Isthmus palaeogeography and the evolution of the connection with the Aegean Sea

Sequence 1 records a transition from deep lacustrine to shallow marine water during a 'transgression': that is, from a lacustrine to a marine environment. This setting requires two conditions: (1) a fault-related opening of the marine connection (i.e. a 'deepening' at the site of the connection, probably not located in the Corinth Isthmus) when (2) the lake level was above the sea level, which is common. If these conditions are met, the active faulting connection can reduce the bathymetry of the basin and establish a marine environment. This opening may be associated at the rift scale with the *c.* 1.8 Ma marine transgression and migration of the Gilbert-type deltas towards the north (Ford *et al.* 2016) and the regression of the southern coast (Rohais and Moretti 2017). This stage corresponds with the transition from Lower/Phase 1 to Middle/Phase 2 of the rift evolution (Ford *et al.* 2016; Nixon *et al.* 2016; Gawthorpe *et al.* 2018).

Sequence 2 is associated with MTDs and soil formations. The dating of conglomerates above (FA6 in sequence 3) at *c.* 300 ka (Collier 1990) implies a large time gap in the sedimentary section. This time gap is locally represented in the geological record by the observed palaeosol (FA5). Regionally, this period corresponds to the beginning of the Peloponnesus uplift. Since *c.* 600 ka, regular *c.* 100 kyr eustatic reconnections to the sea have also been recorded by marine terraces (de Gelder *et al.* 2019) and in deep International Ocean Discovery Program (IODP) cores (McNeill *et al.* 2019) but are not preserved in the study area.

The syntectonic Sequence 3 was built by the tidal strait (FA6) during MIS 9–MIS 8 (337–300 ka: Collier 1990), and records the connection between the Gulf and the Sea in the canal area. Previously, Collier and Thompson (1991) proposed that this connection was located southwards and that the canal area was a strait margin characterized by beach to shoreface deposits. They based their interpretations on the NW-dipping sets of conglomerates, associated with climbing dunes that were interpreted as storm berms. Collier (1990) also reported convex-up surfaces with complex internal structures of scour surfaces, ripple cosets and bundled trough cross-stratification. Collier (1990) explained the NW- and SE-dipping sets as consisting of shoreward- and seaward-migrating bar forms that might reflect minor changes in the relative base level. Collier's interpretation implied SW and NE longshore currents, perpendicular to the canal section. These current directions are quite unusual when the NW–SE-orientated gateway that connected the Corinth Gulf and the Aegean Sea is considered (Fig. 1). Along this gateway, the tidal currents are expected to be parallel to, or close to, its NW–SE orientation but not perpendicular to it (see the previous subsection on the dune-bedded strait zones). In addition, their interpretation of the canal area as a strait margin contradicts the fact that it is the lowest topographical

region connecting the Gulf of Corinth and the Aegean Sea (0–70 m: Fig. 1). Consequently, we question this previous palaeogeographical interpretation as a palaeoshore that required a topographical inversion not supported by the present-day fault network or the facies associations. The coarse-grained dune deposits in the canal (FA6) must imply a lower erosional rate in the canal than for the fine-grained deposits in the south and so prevent a topographical inversion by erosion.

At the same time, in the Corinth Isthmus area, other linear and transverse oolitic dunes have been documented (Fig. 1) (Collier and Thompson 1991; Hayward 1996, 2003, 2013). The ancient Corinth transverse dunes are embedded in the *c.* 240 ka marine terrace 'Old Corinth (II)' at an elevation of *c.* 64 m (Fig. 1) (de Gelder *et al.* 2019). The linear dune at Examilia is part of the *c.* 326 ka 'Temple (II)' marine terrace, at an elevation between *c.* 80 m (in the SW) to *c.* 110 m (in the NW: Fig. 1) (de Gelder *et al.* 2019). The transverse dunes near the Aegean coast are undated and crop out 60–120 m above sea level (Fig. 1). The age constraints imply that the linear Examilia dune is associated with the tidal dune complex FA6, and that the transverse dunes are younger (*c.* 240 ka). They are related to different highstands, contrary to the palaeogeographical reconstruction of Collier and Thompson (1991).

Complementary palaeogeographical information is available from the sedimentology of the Examilia dune. Its internal composition, documented by Hayward (1996), shows that its southwestern part is made up of ooids, 300 μm in diameter, without bioclasts or altered mafic rocks from the north. In contrast, its northeastern part contains heterogeneous particles, ranging from 200 to 800 μm in size, with altered mafic rocks from the north as nuclei or uncoated grain and bioclasts: bivalves and gastropods (Hayward 1996). We suggest that the Examilia dune was built up in a shallow marine area by two sediment sources under two reverse directions of flood and ebb tidal currents (Collier and Thompson 1991). Indeed, the carbonate ooids were generated in shallow carbonate environments that were likely to have been located to the NW, and transported towards the SE. At the same time, the mafic rock nuclei or uncoated particles were derived from the northern Perachora horst by these bidirectional currents (Fig. 1).

Moreover, the Examilia dune crops out at an elevation of between *c.* 80 and *c.* 110 m, so is higher than FA6 in the canal section (*c.* 0–70 m). In reviewing the literature, no fault was found between Examilia and the canal. It can thus be suggested that the Examilia dune formed during the maximum relative sea level during the *c.* 326 ka transgression in a shallow marine area. During the following regression, the canal formed the lowest topographical area and was still flooded, whereas the Examilia dune was exposed to subaerial erosion. The bathymetry at that time in the canal area implies that a narrow lateral constriction was still visible in the topography (Fig. 1). The fault-bounded central horst of the Corinth Canal formed a shallowly submerged sill separating two adjacent depositional areas. The strait deposits (FA6) in the canal would thus result in a fall of the relative base level (i.e. early forced regression: *c.* 300 ka). This hypothesis is also supported by the coarse-grained conglomeratic nature of the large-scale tidal dunes (FA6) that were probably formed during, or close to, the maximum energy state of the strait.

The FA6 strait deposits may also record the reduction in and last connection between the Corinth Gulf and the Aegean Sea. Indeed, the marine Sequence 4 is restricted to the hanging wall of the Kalamaki–Isthmia Fault and is dated at 205 ka (Collier 1990). Likewise, other marine deposits associated with this *c.* 240 ka transgression are localized near the shores of the Corinth Bay and the Aegean Sea (marine terraces and transverse dunes) but not in the centre of Corinth Isthmus (Fig. 1). These findings suggest that during highstands the Gulf of Corinth has been connected to the Ionian Sea to the west since at least since *c.* 240 ka.

Double opening

The FA6 tidal dune architectures record the presence of a strait during MIS 9–MIS 8 (*c.* 300 ka) and attest for strong tidal currents. Within the Mediterranean micro-tidal context, straits can amplify tidal currents by up to 1 m s^{-1}, such as, for example, in the strait centre of the present-day Rion–Antirion Strait located west of the Corinth Gulf (Fourniotis and Horsch 2015; Rubi *et al.* 2022). To reach velocities high enough to build the observed dunes, our hypothesis is that the Corinth Gulf was open both to the west and to the east with an effective connection between the Ionian Sea and the Aegean Sea through the gulf. This double opening could have enhanced the tidal amplification due to the time difference between the tides in the two mentioned seas. Due to the distance separating the two open seas and the usual spread of the tides, a time difference of around 1–2 h can be supposed (Tsimplis 1994). If the Gulf of Corinth had had a double connection, the amplification of tidal currents at the Corinth Strait would have been marked by an increase in the current velocity coming from the Aegean Sea around 1–2 h before the high tide of the Ionian Sea. This hypothesis fits the observation of the tide asymmetry registered by the herringbone cross-bedding in FA6 (Figs 10 & 11). The dominant current coming from the Aegean Sea (SE of the canal

section) was probably responsible for the deposition of the larger and flatter foresets, dipping to the NW, whereas the subordinate weaker current deposited the smaller foresets, dipping to the SE, preserved at the top of the herringbone cross-bedding.

An alternative explanation for the asymmetry is that it could have been generated by the superposition of a unidirectional current on the reversing tidal currents, such as in the Messina Strait (Longhitano 2018*a*). The unidirectional current in the Messina Strait is density driven because of the west-to-east increase in aridity, which generates a west-to-east increase in salinity in Mediterranean Sea (Robinson *et al.* 2001; Schroeder *et al.* 2012). The salinity-driven south-to-north current helps to cause an asymmetry in the sediment transport through the strait (Longhitano 2018*a*).

Conclusions

The aim of the present research was to examine the connections between the Aegean Sea and the Corinth Gulf based on the stratigraphic architecture, sedimentology and structure of the Middle Pleistocene Corinth Canal outcrop. This study has documented two connections: the first recorded by the facies transition from deep lacustrine to shallow marine environments probably triggered by active faulting at *c.* 1.8 Ma (Ford *et al.* 2016; Gawthorpe *et al.* 2018); and the second highlighted a strait system at *c.* 300 ka. This strait is characterized by a fault-bounded strait centre lacking sediments, which probably represented a bypass zone at that time. The two adjacent dune-bedded strait zones preserve coarse-grained cross-beds referable to ancient conglomeratic tidal dunes. This interpretation is based on the following criteria (Longhitano and Chiarella 2020): (i) the opposite dipping directions of the foresets from the central horst; (ii) the simple and compound foreset architectures; and (iii) the lack of mud and the multiscale asymmetrical herringbones cross-stratifications that argue for a dune accretion direction, and tidal currents to the NW and the SE. The sediments that make up the foresets were derived from the erosion of the northern margin and not from the scouring of the strait centre, as occurs in many modern tidal straits. Moreover, the thick set of conglomerates forming the tidal dune complexes in the adjacent strait-centre zone represent an originality of this work, as no previous research has documented facies such as these.

Another remarkable achievement of this study is the reconnection locations between the Gulf of Corinth and the Aegean Sea. Despite the marine terraces having recorded six highstands in the Bay of Corinth (MISs 15e, 13c, 11c, 9c, 7e and 5e: de Gelder *et al.* 2019), the canal outcrop has only recorded the connection at *c.* 300 ka (*c.* MIS 9–MIS 8?: Collier 1990) by a tidal strait. Until this study, the marine connections (MISs 15e, 13c, 11c, 9c, 7e and 5e) were systematically inferred to have occurred through the canal area. Further research should also be carried out to establish the evolution of the connection between the Corinth Rift and the Aegean Sea with emphasis on the Alkyonides Gulf and the Megara Basin. Moreover, we suggest a dual opening – that is, at the eastern and western tips of the gulf – that generated a tidal flow strong enough to form conglomeratic tidal dunes during at least MIS 9c. Since then (MIS 7e and 5e) the connection with the sea would have occurred at the western tip of the Corinth Gulf through the modern Rion Strait. A natural progression of this work is to investigate this western Rion Strait and to model the amplification of the tidal currents.

Acknowledgements We are grateful to Florent Poux, who supported the processing of the photogrammetric model. We are also grateful to Remy Deschamps and Julien Schmitz from IFP Energies Nouvelles, who provided us with a research licence to use 'Virtuoso' (IFPEN): a prototype software dedicated to 3D object interpretation, specifically used in geosciences to interpret 3D outcrop models derived from photogrammetry. We wish to thank Mr George Zouglis, General Manager of the Corinth Canal SA-AEDIK, for the drone and the field permit to conduct this survey. We also thank Sarah Robinet for helpful comments and spelling corrections. We thank Bob Dalrymple, Becky Dorsey and Sergio Longhitano for their very helpful reviews and comments that improved the paper.

Author contributions **BC**: formal analysis (lead), investigation (lead), software (lead), writing – original draft (equal); **RR**: formal analysis (supporting), investigation (supporting), methodology (supporting), resources (supporting), supervision (lead), writing – original draft (equal); **AH-F**: funding acquisition (lead), project administration (lead), resources (lead), supervision (supporting), validation (supporting), writing – original draft (supporting), writing – review & editing (lead).

Funding This work was funded with Fonds de la Recherche Scientifique (FNRS) grant No. PDR T.0123.19 awarded to A. Hubert-Ferrari.

Competing interests The authors declare that they have no known competing financial interests or personal relationships that could have appeared to influence the work reported in this paper.

Data availability The datasets generated during and/or analysed during the current study are not publicly available due to the copyright of the software used to process the photogrammetric models but raw data are available from the corresponding author on reasonable request.

References

Aberhan, M. 2002. Opening of the Hispanic Corridor and Early Jurassic bivalve biodiversity. *Geological Society, London, Special Publications*, **194**, 127–139, https://doi.org/10.1144/GSL.SP.2002.194.01.10

Al-Awwad, S.F. and Pomar, L. 2015. Origin of the rudstone–floatstone beds in the Upper Jurassic Arab-D reservoir, Khurais Complex, Saudi Arabia. *Marine and Petroleum Geology*, **67**, 743–768, https://doi.org/10.1016/j.marpetgeo.2015.05.014

Armijo, R., Meyer, B., King, G., Rigo, A. and Papanastassiou, D. 1996. Quaternary evolution of the Corinth Rift and its implications for the Late Cenozoic evolution of the Aegean. *Geophysical Journal International*, **126**, 11–53, https://doi.org/10.1111/j.1365-246X.1996.tb05264.x

Ashley, G.M. 1990. Classification of large-scale subaqueous bedforms; a new look at an old problem. *Journal of Sedimentary Research*, **60**, 160–172, https://doi.org/10.2110/jsr.60.160

Barnard, P.L., Hanes, D.M., Rubin, D.M. and Kvitek, R.G. 2006. Giant sand waves at the mouth of San Francisco Bay. *Eos, Transactions of the American Geophysical Union*, **87**, 285–289, https://doi.org/10.1029/2006EO290003

Barrier, P. 1984. *Evolution tectono-sédimentaire pliocène et pléistocène du détroit de Messine (Italie)*. PhD thesis, Université d'Aix-Marseille, Marseille, France.

Beckers, A., Beck, C. *et al*. 2016. Influence of bottom currents on the sedimentary processes at the western tip of the Gulf of Corinth, Greece. *Marine Geology*, **378**, 312–332, https://doi.org/10.1016/j.margeo.2016.03.001

Bell, R.E., McNeill, L.C., Bull, J.M. and Henstock, T.J. 2008. Evolution of the offshore western Gulf of Corinth. *Geological Society of America Bulletin*, **120**, 156–178, https://doi.org/10.1130/B26212.1

Briole, P., Rigo, A. *et al*. 2000. Active deformation of the Corinth rift, Greece: Results from repeated Global Positioning System surveys between 1990 and 1995. *Journal of Geophysical Research: Solid Earth*, **105**, 25605, https://doi.org/10.1029/2000JB900148

Collier, R.E.Ll. 1990. Eustatic and tectonic controls upon Quaternary coastal sedimentation in the Corinth Basin, Greece. *Journal of the Geological Society, London*, **147**, 301–314, https://doi.org/10.1144/gsjgs.147.2.0301

Collier, R.E.Ll. and Dart, C.J. 1991. Neogene to Quaternary rifting, sedimentation and uplift in the Corinth Basin, Greece. *Journal of the Geological Society, London*, **148**, 1049–1065, https://doi.org/10.1144/gsjgs.148.6.1049

Collier, R. and Thompson, J. 1991. Transverse and linear dunes in an Upper Pleistocene marine sequence, Corinth. *Sedimentology*, **38**, 1021–1040, https://doi.org/10.1111/j.1365-3091.1991.tb00369.x

Costello, W.R. and Southard, J.B. 1981. Flume experiments on lower-flow-regime bed forms in coarse sand. *Journal of Sedimentary Research*, **51**, 849–864.

Dalrymple, R.W. 2022. A review of the morphology, physical processes and deposits of modern straits. *Geological Society, London, Special Publications*, **523**, https://doi.org/10.1144/SP523-2021-76

Dalrymple, R.W. and Rhodes, R.N. 1995. Estuarine dunes and bars. *In*: Perillo, G.M.E. (ed.) *Geomorphology and Sedimentology of Estuaries*. Developments in Sedimentology, **53**. Elsevier, Amsterdam, 359–422, https://doi.org/10.1016/S0070-4571(05)80033-0

Dalrymple, R.W., Zaitlin, B.A. and Boyd, R. 1992. Estuarine facies models; conceptual basis and stratigraphic implications. *Journal of Sedimentary Research*, **62**, 1130–1146, https://doi.org/10.1306/D4267A69-2B26-11D7-8648000102C1865D

Dalrymple, R.W., Mackay, D.A., Ichaso, A.A. and Choi, K.S. 2012. Processes, morphodynamics, and facies of tide-dominated estuaries. *In*: Davis, R., Jr and Dalrymple, R. (eds) *Principles of Tidal Sedimentology*. Springer, Dordrecht, The Netherlands, 79–107, https://doi.org/10.1007/978-94-007-0123-6_5

de Gelder, G., Fernández-Blanco, D. *et al*. 2019. Lithospheric flexure and rheology determined by climate cycle markers in the Corinth Rift. *Scientific Reports*, **9**, 4260, https://doi.org/10.1038/s41598-018-36377-1

Ferranti, L., Monaco, C., Morelli, D., Tonielli, R., Tortorici, L. and Badalini, M. 2008. Morphostructural setting and active faults in the Messina Strait: new evidence from marine geological data. *Rendiconti Online della Società Geologica Italiana*, **1**, 86–88.

Fernández-Blanco, D., de Gelder, G., Lacassin, R. and Armijo, R. 2019. A new crustal fault formed the modern Corinth Rift. *Earth-Science Reviews*, **199**, 102919, https://doi.org/10.1016/j.earscirev.2019.102919

Ford, M., Williams, E.A., Malartre, F. and Popescu, S. 2009. Stratigraphic architecture, sedimentology and structure of the Vouraikos Gilbert-type fan delta, Gulf of Corinth, Greece. *International Association of Sedimentologists Special Publications*, **38**, 49–90, https://doi.org/10.1002/9781444304411.ch4

Ford, M., Rohais, S., Williams, E.A., Bourlange, S., Jousselin, D., Backert, N. and Malartre, F. 2013. Tectono-sedimentary evolution of the western Corinth rift (Central Greece). *Basin Research*, **25**, 3–25, https://doi.org/10.1111/j.1365-2117.2012.00550.x

Ford, M., Hemelsdaël, R., Mancini, M. and Palyvos, N. 2016. Rift migration and lateral propagation: evolution of normal faults and sediment-routing systems of the western Corinth rift (Greece). *Geological Society, London, Special Publications*, **439**, 131–168, https://doi.org/10.1144/SP439.15

Fourniotis, N.T. and Horsch, G.M. 2015. Baroclinic circulation in the Gulf of Patras (Greece). *Ocean Engineering*, **104**, 238–248, https://doi.org/10.1016/j.oceaneng.2015.04.080

Frey, S.E. and Dashtgard, S.E. 2011. Sedimentology, ichnology and hydrodynamics of strait-margin, sand and gravel beaches and shorefaces: Juan de Fuca Strait, British Columbia, Canada: Strait-margin beaches. *Sedimentology*, **58**, 1326–1346, https://doi.org/10.1111/j.1365-3091.2010.01211.x

Gawthorpe, R.L., Leeder, M.R. *et al*. 2018. Tectono-sedimentary evolution of the Plio-Pleistocene Corinth rift, Greece. *Basin Research*, **30**, 448–479, https://doi.org/10.1111/bre.12260

Greb, S.F. and Archer, A.W. 1995. Rhythmic sedimentation in a mixed tide and wave deposit, Hazel Patch sandstone (Pennsylvanian), eastern Kentucky coal field. *Journal of Sedimentary Research*, **65**, 96–106.

Guerra-Garcia, J.M., Cabezas, P., Baeza-Rojano, E., Espinosa, F. and García-Gómez, J.C. 2009. Is the north

side of the Strait of Gibraltar more diverse than the south side? A case study using the intertidal peracarids (Crustacea: Malacostraca) associated to the seaweed *Corallina elongata*. *Journal of the Marine Biological Association of the United Kingdom*, **89**, 387–397, https://doi.org/10.1017/S0025315409002938

Harms, J., Southard, J. and Walker, R. 1982. *Structures and Sequences in Clastic Rocks*. SEPM Short Course Notes, **9**.

Hayward, C.L. 1996. High-resolution provenance determination of construction-stone: A preliminary study of Corinthian oolitic limestone quarries at Examilia. *Geoarchaeology*, **11**, 215–234, https://doi.org/10.1002/(SICI)1520-6548(199605)11:3<215::AID-GEA2>3.0.CO;2-6

Hayward, C.L. 2003. Geology of Corinth: The Study of a Basic Resource. *Corinth*, **20**, 15, https://doi.org/10.2307/4390714

Hayward, C.L. 2013. Corinthian stone exploitation and the interpretation of inscribed building accounts. *In*: Niemeier, W.-D. (ed.) *The Corinthia and the Northeast Peloponnesus: Topography and History from Prehistoric Times Until the End of Antiquity*. Himler, Munich, Germany, 63–78.

Isla, M.F., Schwarz, E. and Veiga, G.D. 2020. Record of a nonbarred clastic shoreline. *Geology*, **48**, 338–342, https://doi.org/10.1130/G46800.1

James, N.P. and Dalrymple, R.W. 2010. *Facies Models 4*. Geological Association of Canada, St John's, Newfoundland, Canada, https://gac.ca/product/facies-models-4/

Krijgsman, W., Capella, W. *et al*. 2018. The Gibraltar corridor: Watergate of the Messinian salinity crisis. *Marine Geology*, **403**, 238–246, https://doi.org/10.1016/j.margeo.2018.06.008

Lamarche, G., Lurton, X., Verdier, A.-L. and Augustin, J.-M. 2011. Quantitative characterisation of seafloor substrate and bedforms using advanced processing of multibeam backscatter – Application to Cook Strait, New Zealand. *Continental Shelf Research*, **31**, S93–S109, https://doi.org/10.1016/j.csr.2010.06.001

Longhitano, S.G. 2011. The record of tidal cycles in mixed silici-bioclastic deposits: examples from small Plio-Pleistocene peripheral basins of the microtidal Central Mediterranean Sea. *Sedimentology*, **58**, 691–719, https://doi.org/10.1111/j.1365-3091.2010.01179.x

Longhitano, S.G. 2013. A facies-based depositional model for ancient and modern, tectonically-confined tidal straits. *Terra Nova*, **25**, 446–452, https://doi.org/10.1111/ter.12055

Longhitano, S.G. 2018*a*. Between Scylla and Charybdis (part 1): the sedimentary dynamics of the modern Messina Strait (central Mediterranean) as analogue to interpret the past. *Earth-Science Reviews*, **185**, 259–287, https://doi.org/10.1016/j.earscirev.2018.06.008

Longhitano, S.G. 2018*b*. Between Scylla and Charybdis (part 2): The sedimentary dynamics of the ancient, Early Pleistocene Messina Strait (central Mediterranean) based on its modern analogue. *Earth-Science Reviews*, **179**, 248–286, https://doi.org/10.1016/j.earscirev.2018.01.017

Longhitano, S.G. and Chiarella, D. 2020. Tidal straits: basic criteria for recognizing ancient systems from the rock record. *In*: Scarselli, N., Adam, J., Chiarella, D., Roberts, D.G. and Bally, A.W. (eds) *Regional Geology and Tectonics*. 2nd edn. Elsevier, Amsterdam, 365–415, https://doi.org/10.1016/B978-0-444-64134-2.00014-6

Longhitano, S. and Colella, A. 2007. Geomorphology, sedimentology and recent evolution of the anthropogenically modified Simeto River delta system (eastern Sicily, Italy). *Sedimentary Geology*, **194**, 195–221, https://doi.org/10.1016/j.sedgeo.2006.06.004

Longhitano, S.G. and Nemec, W. 2005. Statistical analysis of bed-thickness variation in a Tortonian succession of biocalcarenitic tidal dunes, Amantea Basin, Calabria, southern Italy. *Sedimentary Geology*, **179**, 195–224, https://doi.org/10.1016/j.sedgeo.2005.05.006

Longhitano, S.G. and Steel, R.J. 2016. Deflection of the progradational axis and asymmetry in tidal seaway and strait deltas: insights from two outcrop case studies. *Geological Society, London, Special Publications*, **444**, 141–172, https://doi.org/10.1144/SP444.8

Lowe, D.R. 1982. Sediment Gravity Flows : II. Depositional Models with Special Reference to the Deposits of High-Density Turbidity Currents. *SEPM Journal of Sedimentary Research*, **52**, 279–297, https://doi.org/10.1306/212F7F31-2B24-11D7-8648000102C1865D

Malartre, F., Ford, M. and Williams, E.A. 2004. Preliminary biostratigraphy and 3D geometry of the Vouraikos Gilbert-type fan delta, Gulf of Corinth, Greece. *Comptes Rendus Geoscience*, **336**, 269–280, https://doi.org/10.1016/j.crte.2003.11.016

Martín, J.M., Braga, J.C. and Betzler, C. 2001. The Messinian Guadalhorce corridor: the last northern, Atlantic–Mediterranean gateway. *Terra Nova*, **13**, 418–424, https://doi.org/10.1046/j.1365-3121.2001.00376.x

Martín, J.M., Braga, J.C., Aguirre, J. and Puga-Bernabéu, Á. 2009. History and evolution of the North-Betic Strait (Prebetic Zone, Betic Cordillera): A narrow, early Tortonian, tidal-dominated, Atlantic–Mediterranean marine passage. *Sedimentary Geology*, **216**, 80–90, https://doi.org/10.1016/j.sedgeo.2009.01.005

Martín, J.M., Puga-Bernabéu, Á., Aguirre, J. and Braga, J.C. 2014. Miocene Atlantic-Mediterranean seaways in the Betic Cordillera (Southern Spain). *Revista de la Sociedad Geológica de España*, **27**, 175–186, http://hdl.handle.net/10481/42694

McNeill, L.C., Shillington, D.J. *et al*. 2019. High-resolution record reveals climate-driven environmental and sedimentary changes in an active rift. *Scientific Reports*, **9**, 3116, https://doi.org/10.1038/s41598-019-40022-w

Miall, A.D. 2006. *The Geology of Fluvial Deposits*. Springer, Berlin, https://doi.org/10.1007/978-3-662-03237-4

Montenat, C., Barrier, P. and Di Geronimo, I. 1987. The Strait of Messina, past and present: a review. *Documents et travaux de l'Institut géologique Albert de Lapparent*, **11**, 7–13.

Moretti, I., Sakellariou, D., Lykousis, V. and Micarelli, L. 2003. The Gulf of Corinth: an active half graben? *Journal of Geodynamics*, **36**, 323–340, https://doi.org/10.1016/S0264-3707(03)00053-X

Mulder, T. and Alexander, J. 2001. The physical character of subaqueous sedimentary density flow and their deposits. *Sedimentology*, **48**, 269–299, https://doi.org/10.1046/j.1365-3091.2001.00360.x

Nemec, W. 2009. What is a hyperconcentrated flow. *27th IAS Meeting of Sedimentology*, 20–23 September 2009, Alghero Italy, 20–24.

Nemec, W. and Steel, R.J. 1984. Alluvial and coastal conglomerates: their significant features and some comments on gravelly mass-flow deposits. *Sedimentology of Gravels and Conglomerates*, **10**, 1–31.

Nicholls, E.L. and Russell, A.P. 1990. Paleobiogeography of the Cretaceous Western Interior Seaway of North America: the vertebrate evidence. *Palaeogeography, Palaeoclimatology, Palaeoecology*, **79**, 149–169, https://doi.org/10.1016/0031-0182(90)90110-S

Nixon, C.W., McNeill, L.C. *et al*. 2016. Rapid spatiotemporal variations in rift structure during development of the Corinth Rift, central Greece: Rapid changes in rift structure, Corinth. *Tectonics*, **35**, 1225–1248, https://doi.org/10.1002/2015TC004026

Nugraha, H.D., Jackson, C.A.L., Johnson, H.D. and Hodgson, D.M. 2020. Lateral variability in strain along the toewall of a mass transport deposit: a case study from the Makassar Strait, offshore Indonesia. *Journal of the Geological Society, London*, **177**, 1261–1279, https://doi.org/10.1144/jgs2020-071

Olariu, C., Steel, R.J., Dalrymple, R.W. and Gingras, M.K. 2012. Tidal dunes versus tidal bars: The sedimentological and architectural characteristics of compound dunes in a tidal seaway, the lower Baronia Sandstone (Lower Eocene), Ager Basin, Spain. *Sedimentary Geology*, **279**, 134–155, https://doi.org/10.1016/j.sedgeo.2012.07.018

Ori, G.G. 1989. Geologic history of the extensional basin of the Gulf of Corinth (?Miocene–Pleistocene), Greece. *Geology*, **17**, 918–921, https://doi.org/10.1130/0091-7613(1989)017<0918:GHOTEB>2.3.CO;2

Pallikarakis, A., Triantaphyllou, M.V., Papanikolaou, I., Dimiza, M.D., Reicherter, K. and Migiros, G. 2018. Age constraints and paleoenvironmental interpretation of a borehole sedimentary sequence along the eastern part of the Corinth Isthmus, Greece. *Journal of Coastal Research*, **34**, 602–617, https://doi.org/10.2112/JCOASTRES-D-16-00191.1

Papanikolaou, I.D., Triantaphyllou, M., Pallikarakis, A. and Migiros, G. 2015. Active faulting at the Corinth Canal based on surface observations, borehole data and paleoenvironmental interpretations. Passive rupture during the 1981 earthquake sequence? *Geomorphology*, **237**, 65–78, https://doi.org/10.1016/j.geomorph.2014.10.036

Pemberton, S.G., MacEachern, J.A., Dashtgard, S.E., Bann, K.L., Gingras, M.K. and Zonneveld, J.-P. 2012. Shorefaces. *Developments in Sedimentology*, **64**, 563–603, https://doi.org/10.1016/B978-0-444-53813-0.00019-8

Perissoratis, C., Piper, D.J.W. and Lykousis, V. 2000. Alternating marine and lacustrine sedimentation during late Quaternary in the Gulf of Corinth rift basin, central Greece. *Marine Geology*, **167**, 391–411, https://doi.org/10.1016/S0025-3227(00)00038-4

Poulimenos, G., Zelilidis, A., Kontopoulos, N. and Doutsos, T. 1993. Geometry of trapezoidal fan deltas and their relationship to extensional faulting along the southwestern active margins of the Corinth rift, Greece. *Basin Research*, **5**, 179–192, https://doi.org/10.1111/j.1365-2117.1993.tb00064.x

Pugh, D.T. 1987. *Tides, Surges and Mean Sea Level: A Handbook for Engineers and Scientists*. John Wiley & Sons, Chichester, UK.

Rebesco, M., Hernández-Molina, F.J., Van Rooij, D. and Waahlin, A. 2014. Contourites and associated sediments controlled by deep-water circulation processes: State-of-the-art and future considerations. *Marine Geology*, **352**, 111–154, https://doi.org/10.1016/j.margeo.2014.03.011

Reynaud, J.-Y. and Dalrymple, R.W. 2012. Shallow-marine tidal deposits. *In*: Davis, R.A., Jr and Dalrymple, R.W. (eds) *Principles of Tidal Sedimentology*. Springer, Dordrecht, The Netherlands, 335–369, https://doi.org/10.1007/978-94-007-0123-6_13

Roberts, G.P., Houghton, S.L. *et al*. 2009. Localization of Quaternary slip rates in an active rift in 10^5 years: An example from central Greece constrained by ^{234}U-^{230}Th coral dates from uplifted paleoshorelines. *Journal of Geophysical Research,* **114**, B10, https://doi.org/10.1029/2008JB005818

Robinson, A.R., Leslie, W.G., Theocharis, A. and Lascaratos, A. 2001. Mediterranean Sea circulation. *In*: Steele, J.H., Thorpe, S.A. and Turekian, K.K. (eds) *Encyclopedia of Ocean Science, Volume 1*. Academic Press, San Diego, CA, 1689–1706.

Rohais, S. and Moretti, I. 2017. Structural and stratigraphic architecture of the Corinth Rift (Greece): An integrated onshore to offshore basin-scale synthesis. *In*: Roure, F., Amin, A.A., Khomsi, S. and Al Garni, M.A.M. (eds) *Lithosphere Dynamics and Sedimentary Basins of the Arabian Plate and Surrounding Areas*. Frontiers in Earth Sciences. Springer, Cham, Switzerland, 89–120, https://doi.org/10.1007/978-3-319-44726-1_5

Rohais, S., Eschard, R., Ford, M., Guillocheau, F. and Moretti, I. 2007. Stratigraphic architecture of the Plio-Pleistocene infill of the Corinth Rift: Implications for its structural evolution. *Tectonophysics*, **440**, 5–28, https://doi.org/10.1016/j.tecto.2006.11.006

Rohais, S., Eschard, R. and Guillocheau, F. 2008. Depositional model and stratigraphic architecture of rift climax Gilbert-type fan deltas (Gulf of Corinth, Greece). *Sedimentary Geology*, **210**, 132–145, https://doi.org/10.1016/j.sedgeo.2008.08.001

Rossi, V., Longhitano, S., Mellere, D., Dalrymple, R., Steel, R., Chiarella, D. and Olariu, C. 2017. Interplay of tidal and fluvial processes in an early Pleistocene, delta-fed, strait margin (Calabria, Southern Italy). *Marine and Petroleum Geology*, **87**, 14–30, https://doi.org/10.1016/j.marpetgeo.2017.02.021

Rubi, R., Rohais, S., Bourquin, S., Moretti, I. and Desaubliaux, G. 2018. Processes and typology in Gilbert-type delta bottomset deposits based on outcrop examples in the Corinth Rift. *Marine and Petroleum Geology*, **92**, 193–212, https://doi.org/10.1016/j.marpetgeo.2018.02.014

Rubi, R., Hubert-Ferrari, A. *et al*. 2022. Hydrodynamics and sedimentary processes in the modern Rion strait (Greece): Interplay between tidal currents and internal tides. *Marine Geology*, **446**, 106771, https://doi.org/10.1016/j.margeo.2022.106771

Rubin, D.M. and Carter, C.L. 1987. *Cross-Bedding, Bedforms, and Paleocurrents*. SEPM Concepts in Sedimentology and Paleontology, **1**.

Sachpazi, M., Clément, C. *et al*. 2003. Rift structure, evolution, and earthquakes in the Gulf of Corinth, from reflection seismic images. *Earth and Planetary Science Letters*, **216**, 243–257, https://doi.org/10.1016/S0012-821X(03)00503-X

Santoro, V.C., Amore, E., Cavallaro, L., Cozzo, G. and Foti, E. 2002. Sand waves in the Messina strait, Italy. *Journal of Coastal Research*, **36**(sp1), 640–653, https://doi.org/10.2112/1551-5036-36.sp1.640

Schmitz, J., Deschamps, R., Joseph, P., Lerat, O., Doligez, B. and Jardin, A. 2014. From 3D photogrammetric outcrop models to reservoir models: an integrated modelling workflow. *In*: Humair, F., Matasci, B. *et al*. (eds) *Vertical Geology, From Remote Sensing to 3D Geological Modelling. Proceedings of the first Vertical Geology Conference, 5–7 February 2014, University of Lausanne, Switzerland*, 143–147.

Schroeder, K., Garcìa-Lafuente, J. *et al*. 2012. Circulation of the Mediterranean Sea and its variability. *In*: Lionello, P. (ed.) *The Climate of the Mediterranean Region: From the Past to the Future*. Elsevier, Amsterdam, 187–256.

Stow, D.A.V., Hernández-Molina, F.J., Llave, E., Sayago-Gil, M., Díaz del Río, V. and Branson, A. 2009. Bedform-velocity matrix: The estimation of bottom current velocity from bedform observations. *Geology*, **37**, 327–330, https://doi.org/10.1130/G25259A.1

Taylor, B., Weiss, J.R., Goodliffe, A.M., Sachpazi, M., Laigle, M. and Hirn, A. 2011. The structures, stratigraphy and evolution of the Gulf of Corinth rift, Greece: Structures, stratigraphy and evolution of GoC. *Geophysical Journal International*, **185**, 1189–1219, https://doi.org/10.1111/j.1365-246X.2011.05014.x

Tsimplis, M. 1994. Tidal oscillations in the Aegean and Ionian Seas. *Estuarine, Coastal and Shelf Science*, **39**, 201–208, https://doi.org/10.1006/ecss.1994.1058

Venditti, J.G., Church, M. and Bennett, S.J. 2005. On the transition between 2D and 3D dunes. *Sedimentology*, **52**, 1343–1359, https://doi.org/10.1111/j.1365-3091.2005.00748.x

von Freyberg, B. 1973. *Geologie des Isthmus von Korinth*. Erlanger geologische Abhandlungen, **95**.

Weill, P., Mouazé, D. and Tessier, B. 2013. Internal architecture and evolution of bioclastic beach ridges in a megatidal chenier plain: Field data and wave flume experiment. *Sedimentology*, **60**, 1213–1230, https://doi.org/10.1111/sed.12027